AD-A179 654 ON THE UNSTEADY CHARACTERISTICS OF FLOWS AROUND AN NACA 1/1
0012 AIRFOIL..(U) MASSACHUSETTS INST OF TECH CAMBRIDGE
CENTER FOR AERODYNAMIC S.. E E COVERT ET AL. JAN 86
UNCLASSIFIED 86-1 AFOSR-TR-87-0396 AFOSR-80-0282 F/G 20/4 NL

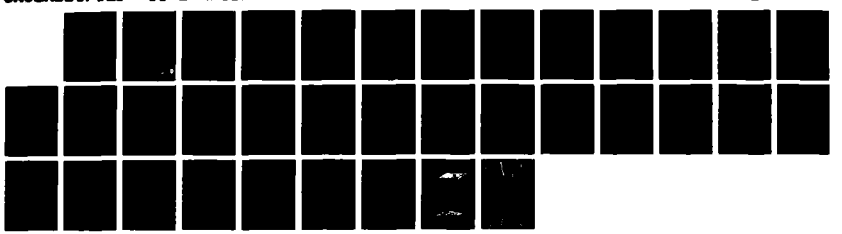

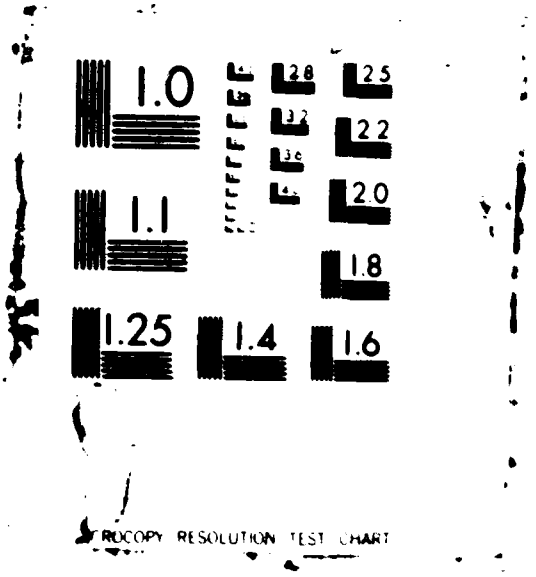
1.0
1.1
1.25
1.4
1.6
2.0
2.2
2.5
1.8
ROCOPY RESOLUTION TEST CHART

UNCLASSIFIED

DTIC FILE COPY (2)

SECURITY CLASSIFICATION OF THIS PAGE

AD-A179 654

1a REPORT SECURITY CLASSIFICATION UNCLASSIFIED	1b RESTRICTIVE MARKINGS
2a SECURITY CLASSIFICATION AUTHORITY	3 DISTRIBUTION/AVAILABILITY OF REPORT APPROVED FOR PUBLIC RELEASE DISTRIBUTION IS UNLIMITED
2b DECLASSIFICATION/DOWNGRADING SCHEDULE	
4 PERFORMING ORGANIZATION REPORT NUMBER(S)	5 MONITORING ORGANIZATION REPORT NUMBER(S) AFOSR-TR- 87-0396
6a NAME OF PERFORMING ORGANIZATION MASSACHUSETTS INST OF TECH	6b OFFICE SYMBOL (If applicable)
6c ADDRESS (City, State and ZIP Code) MASSACHUSETTS INST OF TECH 77 MASSACHUSETTS AVE, RM 31-702 CAMBRIDGE, MA 02139	7a NAME OF MONITORING ORGANIZATION AFOSR/NA 7b ADDRESS (City, State and ZIP Code) BUILDING 410 BOLLING AFB, DC 20332-6448
8a NAME OF FUNDING/SPONSORING ~~ORGANIZATION~~ AFOSR/NA	8b OFFICE SYMBOL (If applicable) NA
8c ADDRESS (City, State and ZIP Code) BUILDING 410 BOLLING AFB, DC 20332-6448	9 PROCUREMENT INSTRUMENT IDENTIFICATION NUMBER AFOSR-80-0282
	10 SOURCE OF FUNDING NOS

PROGRAM ELEMENT NO	PROJECT NO	TASK NO.	WORK UNIT NO.
~~2307~~ 61102F	~~A2~~ 2307	A2	

11 TITLE (Include Security Classification)
(U) ON THE UNSTEADY CHARACTERISTICS OF FLOWS AROUND AN NACA 0012 AIRFOIL

12 PERSONAL AUTHOR(S)
E. COVERT

13a TYPE OF REPORT	13b TIME COVERED	14 DATE OF REPORT (Yr, Mo, Day)	15 PAGE COUNT
FINAL REPORT	FROM _____ TO _____	JANUARY 1986	33

16 SUPPLEMENTARY NOTATION

17 COSATI CODES			18 SUBJECT TERMS (Continue on reverse if necessary and identify by block number)
FIELD	GROUP	SUB GR	UNSTEADY FLOWS, DYNAMIC STALL, SEPARATED FLOWS

19 ABSTRACT (Continue on reverse if necessary and identify by block number)

Unsteady excitation was generated by a rotating eliptical cylinder located below and behind the airfoil. This produced an unsteady flow of approximately constant phase. Four regions were identified within the unsteady turbulent boundary layer and the viscous sublayer was most affected by the unsteady flow. The velocity phase shift was found to be a function of the reduced frequency of the rotating eliptical cylinder. This phenomena was examined experimentally and analytically.

20 DISTRIBUTION/AVAILABILITY OF ABSTRACT	21 ABSTRACT SECURITY CLASSIFICATION
UNCLASSIFIED/UNLIMITED ☐ SAME AS RPT ☐ DTIC USERS ☐	UNCLASSIFIED

22a NAME OF RESPONSIBLE INDIVIDUAL	22b TELEPHONE NUMBER (Include Area Code)	22c OFFICE SYMBOL
HENRY E HELIN, CAPTAIN, USAF	202-767-4935	AFOSR/NA

DD FORM 1473, 83 APR EDITION OF 1 JAN 73 IS OBSOLETE

UNCLASSIFIED

CENTER FOR AERODYNAMIC STUDIES

Report 86-1

January 1986

ON THE UNSTEADY CHARACTERISTICS OF FLOWS AROUND AN NACA 0012 AIRFOIL

Eugene E. Covert
Michael J. Fletcher
Kirk J. Flittie
Samuel W. Linton

FINAL REPORT ON GRANT 80-0282

Submitted to

Dr. James McMichael, Program Manager
Mechanics Branch
Air Force Office of Scientific Research
Bolling AFB, District of Columbia 20332

I N T R O D U C T I O N

Research under contract F4920-79-26 began in 1978 with the intent of gaining a better understanding of the aerodynamic behavior of unsteady flows. The unsteady excitation was generated by a rotating elliptical cylinder located below and behind the airfoil. This produced an unsteady flow of essentially constant phase. Since 1978, testing has been performed with reduced frequency, based on half chord, varying from 0 (steady flow) to 6.4. The Reynolds number varied from 375,000 to 1,400,000, but most of the testing was conducted at a Reynolds number of 700,000. The metric surface used was a NACA 0012 airfoil, of 20 inch span and chord, which was set between two sidewalls to ensure two-dimensionality. The details of instrumentation are shown in figures 1 and 2 and described in depth in references 1, 2 and 3. The unsteady data taken during a test is separated into three parts: a time invariant mean part; a periodic part of zero mean, but not necessarily sinusodial; and the remainder which has zero mean and is not periodic.

$$f = \bar{f} + \tilde{f} + f'$$

signal = time mean + periodic + remainder

The ensemble average is defined as

$$\underset{\text{ensemble average at a fixed phase}}{\langle f \rangle} = 1/N \sum_{n=1}^{N} f_n = \tilde{f} + \bar{f}$$

The time invariant part, or time mean part, $\bar{f}$, is the time average over a cycle. The periodic part, $\tilde{f}$, is the ensemble average of the cycles less the time mean. The remainder, f', is the difference between the signal and the ensemble average, and is assumed turbulent.

Each year since work began in 1978, a number of significant

accomplishments have been made. Work began in 1978 with studies of turbulent boundary layers on a flat plate; pressure distributions on the NACA 0012 airfoil in steady flow; and steady boundary layers at zero angle of attack [4,5]. In 1979, the unsteady flow field was studied by measuring the excitation velocities induced by the rotating ellipse [6]. In 1980 we began the first extensive effort to measure the unsteady surface pressures and velocity profiles of the boundary layer on the airfoil at zero angle of attack [6]. Continued surface pressure measurements and boundary layer profiles were taken in 1981 with the angle of attack varying up to 15 degrees [3]. Wake measurements, two-dimensionality tests and numerical boundary layer calculations were performed in 1982 and continued through 1983 [3]. Also beginning in 1983 were studies of the surface pressures in separated flow [7]. Wall shear measurements began in 1984 with the initial design of the hot wire shear probe and the hot film tests.

There were two major accomplishments made during the last year: first, we were successful in constructing and testing a hot wire type surface mounted shear probe; and second, we were able to use a traveling wave excitation to generate the unsteady flow.

The work done by P. F. Lorber [3] for his Ph.D. thesis included extensive analysis of the surface pressures and boundary layers on an NACA 0012 airfoil, but he could only estimate the wall shear from the velocity profiles of the boundary layer. To gain a better understanding of the wall shear associated with the NACA 0012 airfoil, a wall shear probe was constructed. The probe is shown in figure 3 and the details of the probe construction can be found in K. J. Flittie's S. M. thesis [1]. This probe, having the high frequency response characteristics of a hot wire type device, enabled us to measure the wall shear directly for steady or unsteady flows.

The other major accomplishment was creating a different type of unsteady perturbation and measuring the induced aerodynamic behavior from it. As noted the initial the unsteady perturbation was created using a rotating elliptical cylinder located below and behind the airfoil (see figures 1 and 2). The result of the airfoil/ellipse combination lead to an essentially constant phase type excitation. This year we were able to generate a traveling wave by means of the gust generators. The gust generators are two parallel airfoils (see figures 4 and 5) which create a periodic circulation. If the circulations of the two generators are in phase, the effective perturbation is in the longitudinal, or streamwise direction. If the circulations are out of phase, the effective perturbation is in the lateral, or spanwise direction. The details of the gust generators performance can be found in reference 8.

T E C H N I C A L A C T I V I T I E S

SHEAR PROBE RESEARCH

An extensive amount of wall shear data, both steady and unsteady was recorded during the last year. What follows is a summary of the significant results obtained by K. J. Flittie and reported in his S. M. thesis [1].

The hot wire shear probe is based on a probe designed by J. Cousteix [9] of ONERA/CERT. Essentially, the probe is a hot wire located flush with the surface (see figure 3). There is a cavity etched into the surface beneath the sensing wire in order to prevent contact, and consequently thermal conduction, with the surface. Thus the probe retains a high dynamic response, which makes it ideal to use in measuring unsteady flows.

To test the integrity of the shear probe, the turbulent wall shear was measured on a flat plate with a zero pressure gradient. The results shown in figure 6 demonstrate that the measurements from the probe were repeatable to

within 10% of the predicted empirical results using boundary layer profiles. It is worth noting that in each case, the measured shear stress was higher than the predicted value. It is believed that this is attributed to surface roughness rather than a property of the probe, as will be discussed below.

A. CONSTANT PHASE EXCITATION WALL SHEAR RESULTS

The wall shear was measured for steady and unsteady flows at the 70%, 85% and 94% chord locations for zero and ten degrees angle of attack and Reynolds number of 700,000. The unsteady cases studied consisted of four different reduced frequencies, 0.5, 1.0, 2.0, and 6.4. Unsteady boundary layer profiles were also taken for the above cases. There were four significant results found during this program:

(1) The time mean velocity profiles, integral parameters and wall shear stresses were the same as in the equivalent steady cases studied.

(2) A quasi-steady Clauser method was developed and found to yield time mean c_f's to within 15% of the experimental c_f's and phase angles within 50 degrees of the experimental phase angles for reduced frequencies of less than 2.

(3) For unsteady flow near the wall, a universal velocity distribution does not appear to exist.

(4) The oscillating adverse pressure gradient has significant influence on the viscous sublayer.

Figures 7 through 10 show the time mean u+ versus y+ curves at zero angle of attack and 85% chord. Note how all the curves are very nearly identical. If we compare these curves to the steady case, figure 11, at zero angle of attack and 85% chord, we find no discernible difference. This same behavior can be seen in the velocity profiles and wall shear.

The method proposed by F. H. Clauser [10] assumes that a universal velocity profile exists near the wall. The method was developed for steady turbulent flow, but we used it in a quasi-steady analysis. The idea is to apply the Clauser technique at various points over a cycle. This assumes that the logarithmic overlap layer is valid at each point in the cycle. It also assumes that the friction velocity, u^*, is the correct scaling parameter for the inner region of the boundary layer and that the velocity phase angle remains constant in the logarimthic region.

The results from the Clauser analysis, shown in figures 12-15, are encouraging. The time mean c_f's from the Clauser technique were within 15% of the predicted the experimental c_f's up to a reduced frequency of approximately 2. The Clauser technique also predicted the phase angles to within 50 degrees of the experimental results.

It appears that of the four regions identified with the turbulent boundary layer, the viscous sublayer is the most effected by an unsteady flow. The velocity phase shift, for example, has been found to be a function of reduced frequency. The general shapes at reduced frequencies of above and below 2 are shown in figure 16 and 17. It is important to note how phase shift changes rapidly at low reduced frequencies as the wall is approached. The hope for a universal velocity distribution is not substantiated since the assumption for such a principle a constant phase shift as the wall is approached, fails.

To analyze the qualitative behavior of the phase shift with reduced frequency, consider a small perturbation expansion. The ensemble average momentum equation is

$$\frac{\partial \langle u \rangle}{\partial t} + \langle u \rangle \frac{\partial \langle u \rangle}{\partial x} + \langle v \rangle \frac{\partial \langle u \rangle}{\partial y} = -\frac{1}{\rho}\frac{\partial \langle p \rangle}{\partial x} + \nu \frac{\partial^2 \langle u \rangle}{\partial y^2} - \frac{\partial \langle u'u' \rangle}{\partial x} - \frac{\partial \langle u'u' \rangle}{\partial y} \qquad (1)$$

Since we are considering flow very near the wall, we neglect the turbulence and convection terms so 1 simpifies to*

$$\frac{\partial \langle u \rangle}{\partial t} = \frac{\partial \langle U_e \rangle}{\partial t} + \langle U_e \rangle \frac{\partial \langle U_e \rangle}{\partial x} + \nu \frac{\partial^2 \langle u \rangle}{\partial y^2} \qquad (2)$$

Where $\bar{U}e(dUe/dx)+dUe/dt$ is from the unsteady Bernoulli equation. We now expand the u components of velocity in a small pertubation parameter, (ε).

$$u(x,y,t) = \bar{u}_o(x,y) + \frac{\varepsilon}{2}\tilde{u}_1(x,y)e^{i(\omega t + \phi_u)} \qquad (3)$$

$$U_e(x,t) = \bar{U}_{e_o}(x) + \frac{\varepsilon}{2}\tilde{U}_{e_1}(x)e^{i(\omega t + \phi_{u_e})} \qquad (4)$$

Substitution 3 and 4 into 2 and collecting powers of (ε) yields

$$O(\varepsilon): \; i\omega \tilde{u}_1 - \nu \frac{\partial^2 \tilde{u}_1}{\partial y^2} = \left[i\omega \tilde{U}_{e_1} + \bar{U}_{e_o} \frac{\partial \tilde{U}_{e_1}}{\partial x} + \tilde{U}_{e_1} \frac{\partial \bar{U}_{e_o}}{\partial x} \right] e^{i(\phi_{u_e} - \phi_u)} \qquad (5)$$

* $\frac{\partial \langle u'v' \rangle}{\partial y}$ is small near the wall since $\frac{\partial}{\partial y}\langle u'v' \rangle \sim -n^2 y^3 \left(\frac{\partial \langle u \rangle}{\partial y}\right) \left| \frac{\partial \langle u \rangle}{\partial y} \right|$

as $y \to 0$ near separation $\langle u \rangle \sim y^2$, so if mixing length is a valid concept the last term is still neglible.

Consider the real part of the first order term

$$\nu \frac{\partial^2 \tilde{u}_1}{\partial y^2} = -\tilde{U}_{e_1} \omega \sin(\phi_{u_e} - \phi_u) + \left[\bar{U}_{e_o} \frac{\partial \tilde{U}_{e_1}}{\partial x} + \tilde{U}_{e_1} \frac{\partial \bar{U}_{e_o}}{\partial x} \right] \cos(\phi_{u_e} - \phi_u) \quad (6)$$

The first term on the right hand side is due to the unsteady external intertia term. The second term on the right hand side is due to the unsteady pressure gradient. For small reduced frequencies, the first term (the inertial effect of the unsteady external velocity) is negligible compared to the unsteady pressure gradient. Clearly, if

$$2k \tan(\phi_{u_e} - \phi_v) << \frac{\partial U_{e_o}}{\partial (x/c)} + \frac{\bar{U}_{e_o}}{\tilde{U}_{e_1}} \frac{\partial \tilde{U}_{e_1}}{\partial (x/c)} \quad (7)$$

the unsteady pressure gradient is the dominant factor in determining the phase shift and amplitude of the velocity near the wall. As the reduced frequency is increased, and if the unsteady external velocity increases, the inertial term becomes significant and effects both the phase shift and amplitude.

B. TRAVELING WAVE EXCITATION WALL SHEAR RESULTS

During the traveling wave testing, the wall shear stress was measured at the same test Reynolds number, 700,000, angles of attack and chord locations, 70%, 85% and 94%. Although we were able to generate both a longitudinal and lateral perturbation, the reduced frequency was limited to 1.5 due to the power limits to drive of the gust generators [8]. The significant results from this test sequence were as follows:

(1) As before, the time mean velocity profiles and wall shear values were

the same as the equivalent steady cases studied.

(2) The lateral perturbation at lower reduced frequencies appears to create locally high pressure gradients which accelerate and decelerate the flow resulting in highly inflected unsteady velocity profiles and an oscillating transition point on the aft portion of the airfoil.

(3) The quasi-steady Clauser method showed a qualitative agreement to the experimental waveform results over a cycle. Quantitatively, as before, the time mean values of cf were within 15% of the experimental values and phase shifts to within 50 degrees.

The time mean curves of U+ versus y+, figures 18-23, demonstrate how the time average parameters correspond to the values of the steady cases. Comparing figures 18-23 to the steady curves shown in figures 11, we find no appreciable differences. Recall, this was the same result found for the constant phase excitation, thus we conclude, this characteristic is independent of the type of excitation.

Although certain characteristics of the unsteady boundary layer flows were independent of the type of excitation, (that is, constant phase versus traveling wave) this was not true for every case. For example, at lower reduced frequencies in the lateral mode, there was a strong indication of locally high pressure gradients and/or laminar to turbulent transition. Figures 24 and 25 show the boundary layer characteristics for the 70% chord position with a lateral mode excitation and reduced frequency of 0.5. Notice that the skin friction coefficient curve, figure 25, is step-like and considerablly smoother between phase angles of 90 and 240 degrees. This is very different than either the longitudinal case (figure 26) or the constant

phase case (figure 27).

Assuming that a quasi-steady analysis is valid at this low reduced frequency, we can examine the flow field at any point in the cycle as if it were steady. A steady turbulent boundary layer velocity profile becomes more highly inflected with increasing adverse pressure gradient, the shape factor increases and the c_f decreases. This behavior is seen in figures 24 and 25 and it appears that the velocity profile oscillates between a fully developed and highly inflected profile on the aft section of the airfoil. In other words, an oscillating transition region and locally high adverse pressure gradients causing highly inflected velocity profiles near the trailing edge may account for the rapid variations seen in the skin friction coefficient, shape factor, and local pressure gradient ensemble average plots.

As in the constant phase excitation analysis, a quasi-steady Clauser technique was used. Figures 28-30 show the comparison between the experimental data at the 70% chord and the quasi-steady Clauser method. The ensemble Clauser wave exhibits a qualitative similarity to the data, with best results at the low reduced frequency. The time mean values from the Clauser method were also within 15% of the time mean experimental values and the phase shifts from the Clauser method were within 50 degrees of the experimental phase angles. This technique proved to be useful for both types of excitations, yielding common results for each case.

UNSTEADY PRESSURE RESULTS USING A TRAVELING WAVE

Four years ago, for his S. M. thesis, P. F. Lorber [6] used unsteady thin airfoil theory to predict surface pressures. By measuring the upwash induced by the unsteady flow along the chord of the airfoil, Lorber calculated the surface pressures using a method developed by Theodorsen. This method assumes

a constant phase excitation, which is the type of flow field generated by the airfoil/ellipse configuration. By mearsuring the surface pressures directly, he was able to compare his theoretical results to the experimental results.

By employing a traveling wave type excitation, Theodorsen's analysis can no longer be used to describe resulting surface pressures. There are two theories which apply to a convected gust (or traveling wave). One is a variation of Theodorsen's method in which the convected gust is accounted for. This method was developed by Von Karman and Sears [11]. The other analysis, developed by Horlock [12] applies to longitudinal gusts over a symetric airfoil at small angles of attack. The results of both of these analysis are described in S. W. Linton's S. M. thesis [2] and will be discussed here.

A. LATERAL GUST RESULTS

For the lateral, or vertical, gust cases, S. W. Linton [2] applied an extended Sears theory. The extended theory accounted for variation of the pressure amplitude over the airfoil chord. Using approximations this theory to model the unsteady flow, Linton was able to estimate the pressure distribution on the airfoil. By comparing the estimated results to the experimental results, he found:

(1) The magnitude and location of the difference pressure amplitude did not model accurately, with the basic theory.

(2) The extended theory predicted phase variations, but of a lower magnetude and more gradual than the data.

Figures 31-34 show the first harmonic of the unsteady difference pressure coefficient, the classical Sears theory prediction, and the extended Sears theory prediction. At the low reduced frequency of 1.5, both theories offer practical results, but as reduced frequency increases, both theories breakdown. The classical theory does not seem to predict any oscillatory behavior above a reduced frequency of 1 to 1.25. Although the extended theory

does predict the oscillations, it fails near the leading edge and trailing edge, particularly at the higher reduced frequencies (see figure 31). This may be due to the fact that phase velocity variations were not modeled.

Figures 35-38 show the phase lags over the chord. According to the classical theory, the phase lag should be constant over the chord, but this was clearly not the case. The extended theory is shows some variation of the phase over the chord is to be expected but, the expected behavior compares badly with the measured behavior of the phase lag. These results seem to indicate that the pressure waves are not moving along the airfoil at constant phase, as predicted by the classical theory.

B. LONGITUDINAL GUST RESULTS

To analyze the longitudinal gust cases, theory by Horlock [12] was used. This is a higher order effect than the vertical gust excitations. In this case, the lift is proportional to the angle of attack times the longitudinal gust amplitude. We see how small this effect is by comparing figures 39 and 40. Figure 39 is the full difference pressure coefficient due to a longitudinal gust at a reduced frequency of 0.5. The unsteadiness is very difficult see, but by subtracting out the mean, as in figure 40, the unsteadiness is clear. Because this effect was smaller than indicated by well to the theory of Horlock.

T E C H N I C A L S U M M A R Y

Research concluded last year under contract F4920-79-026 with further examination of the turbulent boundary layer and surface pressures on an NACA 0012 airfoil subjected to an unsteady flow. There were two types of waveform used in generating the unsteadiness. The first was a constant phase type excitation. This type of waveform was used for most of the unsteady testing.

The second type of waveform was a traveling wave type excitation. Boundary layer profiles, wall shear measurements and surface pressure measurements were taken on the airfoil when subjected to the traveling gust type excitation. The wall shear measurements were successfully made at the 70%, 85% and 94% airfoil chord locations for steady and unsteady flows. Both travel wave and constant phase excitations were used to generate the unsteady flow fields. Boundary layer profiles were also taken at these locations for the purpose of comparing the measured wall shear to the wall shear predicted by a quasi-steady Clauser method. Results were obtained for a Reynolds number of 700,000, and angles of attack of 0 and 10 degrees. At 0 degrees angle of attack, the experimental results were within 15% of the Clauser predictions. At 10 degrees angle of attack, the Clauser method failed to adequately predict the shear.

Two types of linerarized potential thin airfoil theory were used in an attempt to model the traveling wave type excitation. For lateral perturbation cases, the classical Sears' theory and an extended Sears' theory were used. For our excitation, which was far from that assumed by Sears, the classical theory was unable to predict phase or amplitude variations over the airfoil chord. The extended Sears' theory, which allowed for the amplitude variation of the wave as it convects, was able to indicated both phase and amplitude variations, but results ranged from adequate at low reduced frequencies (0.5) to poor at the higher reduced frequencies (1.25-1.5). For longitudinal perturbations, a method developed by Horlock was used. However, the unsteady lift developed is of the order of the angle of attack multiplied by the magnitude of the perturbation, which makes this a small effect. Consequently, our attempt to model the longitudinal gust failed.

I N T E R A C T I O N S

Visitors

Professor H. U. Thomman	ETCH Zurich, Switzerland
Professor Hans Fernholz	Technical University of Berlin Hermann Fottinger Institute
Dr. Richard Margason	Head of Low Speed Aerodynamics NASA/Langley, Langley, VA.
Dr. R. J. Hakkin	Assistant Director Physical Sciences McDonnell-Douglas Research Laboratory St. Louis, MO.

PRESENTATIONS DURING PROJECT

Third Annual Conference on CFD, California State University at Long Beach.

Covert, E.E., Lorber, P.F. and Vaczy, C.M., "Measurements of the Near Wake of an Airfoil in Unsteady Flow," Accepted for presentation as an AIAA Paper 83-0127 at the AIAA 21st Aerospace Sciences Meeting, Reno, Nevada, January 1983.

AIAA 21st Aerospace Science Meeting, January 1983.

AFOSR - University of Colorado - Seiler Hub Workshop, August 1983.

PUBLICATIONS DURING PROJECT

Lorber, P.F. and E.E. Covert, "Unsteady Airfoil Pressures Produced by Periodic Aerodynamic Interference," Submitted to AIAA Journal, February 1981.

Lorber, P.F. and E.E. Covert, "On the Kutta Condition in Unsteady Flow," Submitted to Journal of Fluid Mechanics.

Lorber, P.F. and Covert, E.E., "Unsteady Airfoil Pressures Produced by Periodic Aerodynamic Interference," AIAA Journal, 20, September 1982, pp. 1153-1159.

Covert, E.E. and Lorber, P.F., "Unsteady Turbulent Boundary Layers in Adverse Pressure Gradients," AIAA Paper 82-0966, Submitted to AIAA Journal in July 1982.

THESES AWARDED DURING PROJECT

Kanevsky, A.R.; Comparison of the Pressure Distribution for Circulation Generated by Angle of Attack with that Generated by Trailing Edge Perturbation, S.M. Thesis, Dept. of Aeronautics and Astronautics, MIT, Feb. 1978.

Cervisi, R.T.; Turbulent Boundary Layers on an Airfoil in Several Adverse Pressure Gradients, S.M. Thesis, Dept. of Aeronautics and Astronautics, MIT, Sept. 1978.

Lorber, P.F.; Unsteady Airfoil Pressures Induced by Perturbation of the Trailing Edge Flow, S.M. Thesis, Dept. of Aeronautics and Astronautics, MIT, Feb. 1981.

Cordier, S.J.; Characteristics of an Acoustically Excited Unsteady Boundary Layer in an Adverse Pressure Gradient, S.M. Thesis, Dept. of Naval Architecture and Marine Engineering, MIT, Aug. 1983.

Lorber, P.F.; Turbulent Boundary Layers on an Airfoil in Unsteady Flow, PhD Thesis, Dept. of Aeronautics and Astronautics, MIT, May 1984.

Vaczy, C.M.; Unsteady Separated Flow Fields About a NACA 0012 Airfoil, S.M. Thesis, Dept. of Aeronautics and Astronautics, MIT, May 1984.

Flittie, K.J.; Wall Shear Measurements in an Unsteady Turbulent Boundary Layer, S.M. Thesis, Dept. of Aeronautics and Astronautics, MIT, Sept. 1985.

Linton, S.W.; The Aerodynamics of a NACA 0012 Airfoil in Unsteady Flow, S.M. Thesis, Dept. of Aeronautics and Astronautics, MIT, Sept. 1985.

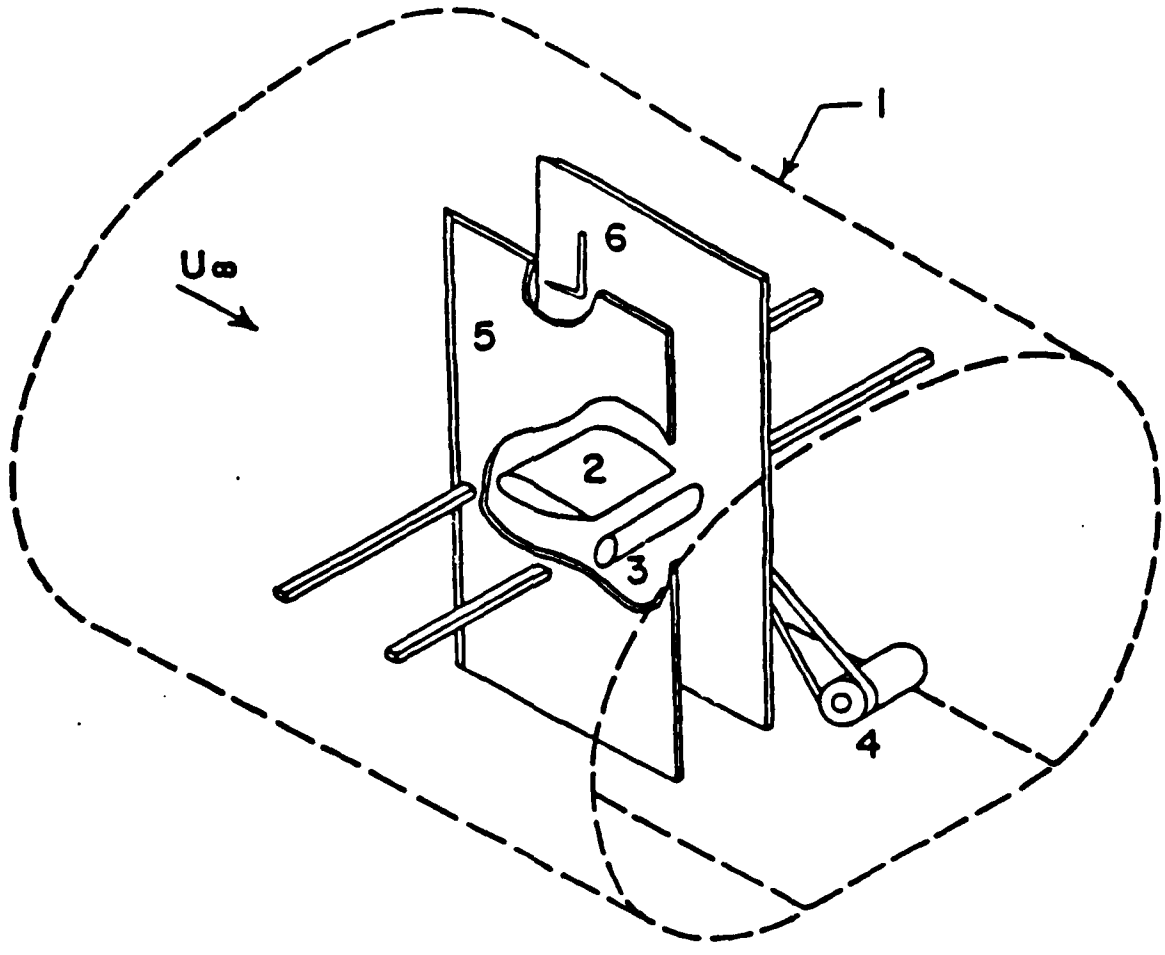

1) Test Section
2) NACA 0012 Airfoil
3) Rotating Elliptic Cylinder
4) Drive Motor (0-3300 rpm)
5) 2-D Sidewalls
6) Pitot-Static Probe

FIGURE 1

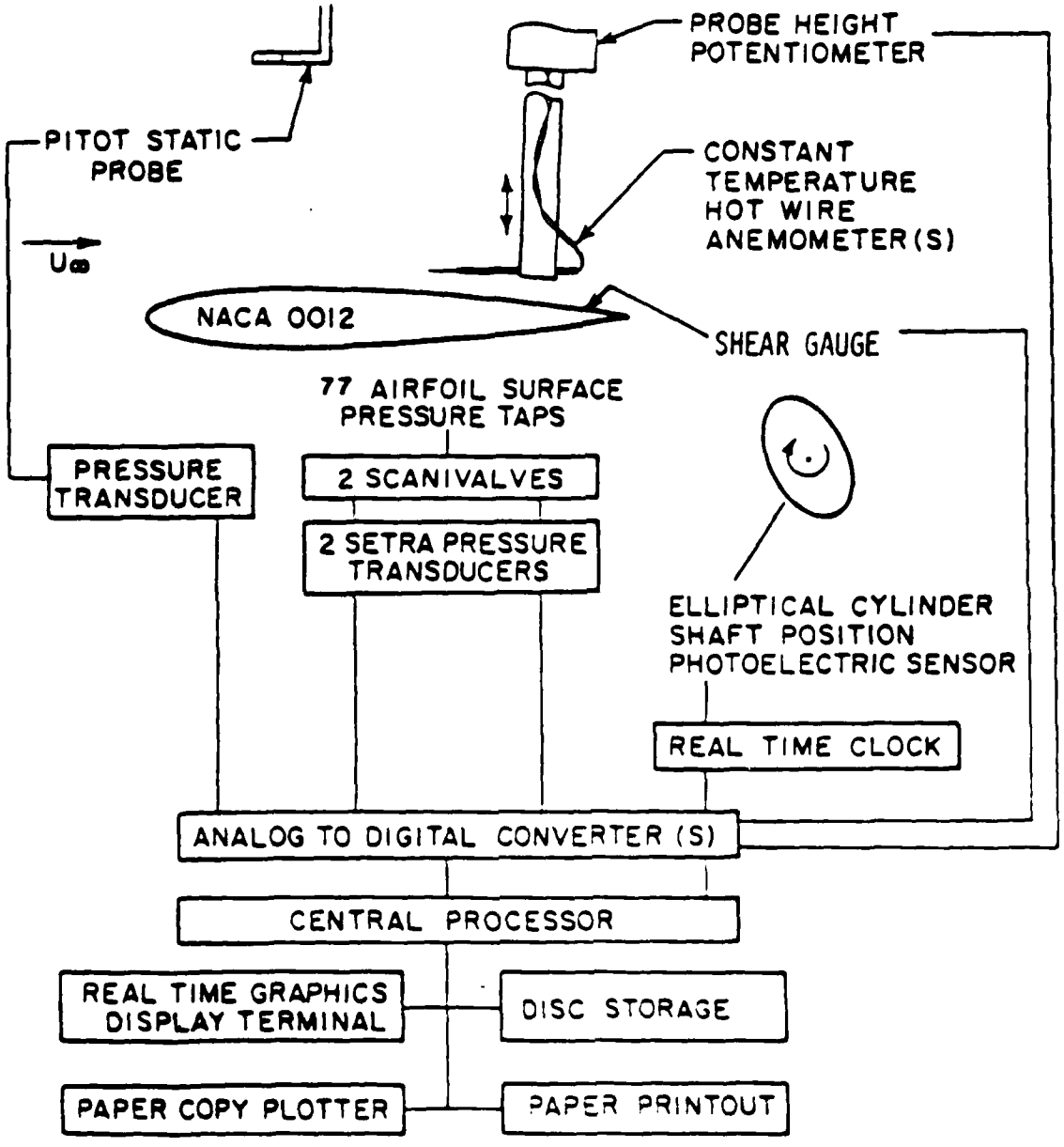

FIGURE 2 EXPERIMENTAL APPARATUS FOR DATA ACQUISITION PROCESS.

SHEAR GAUGE

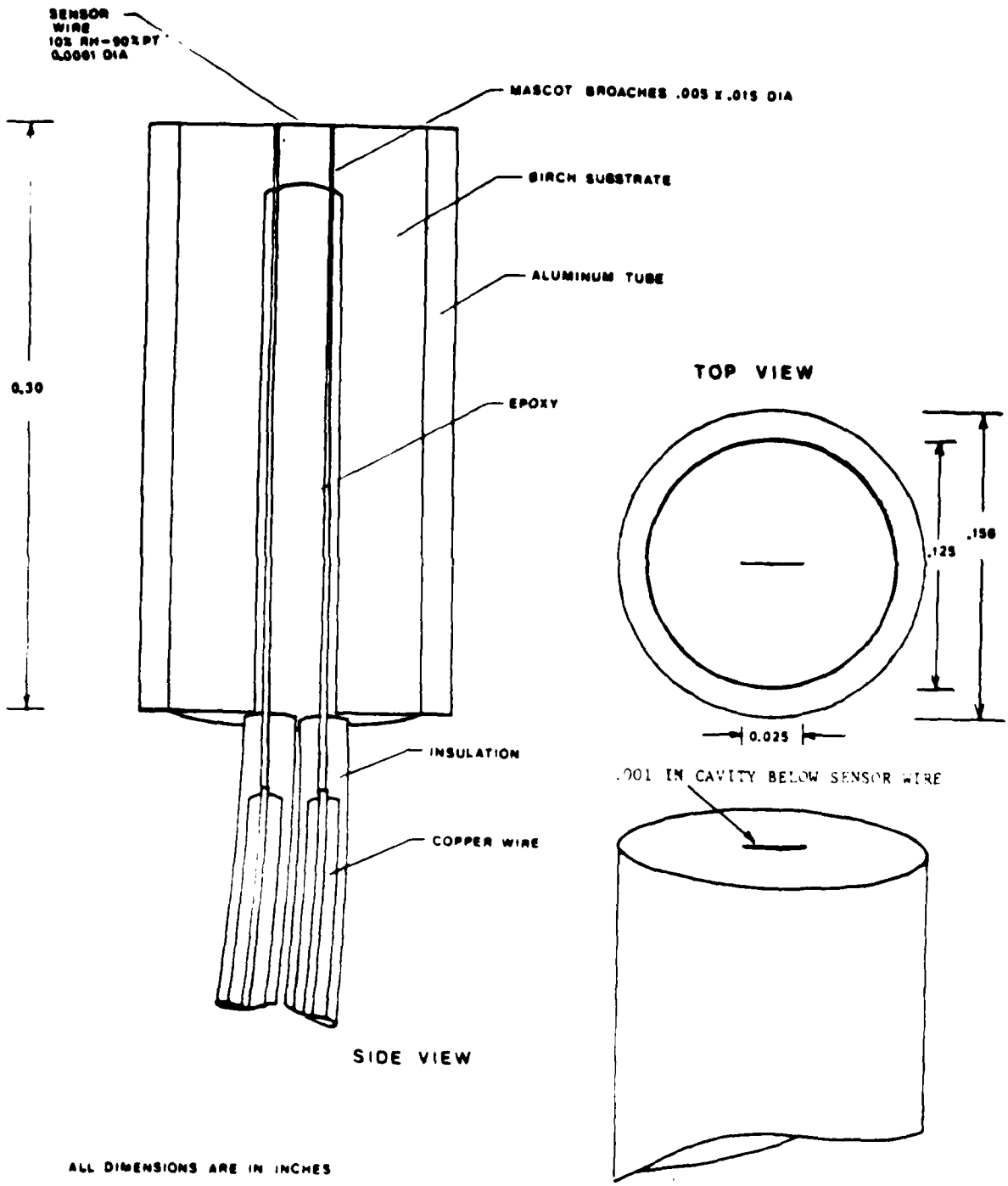

FIGURE 3

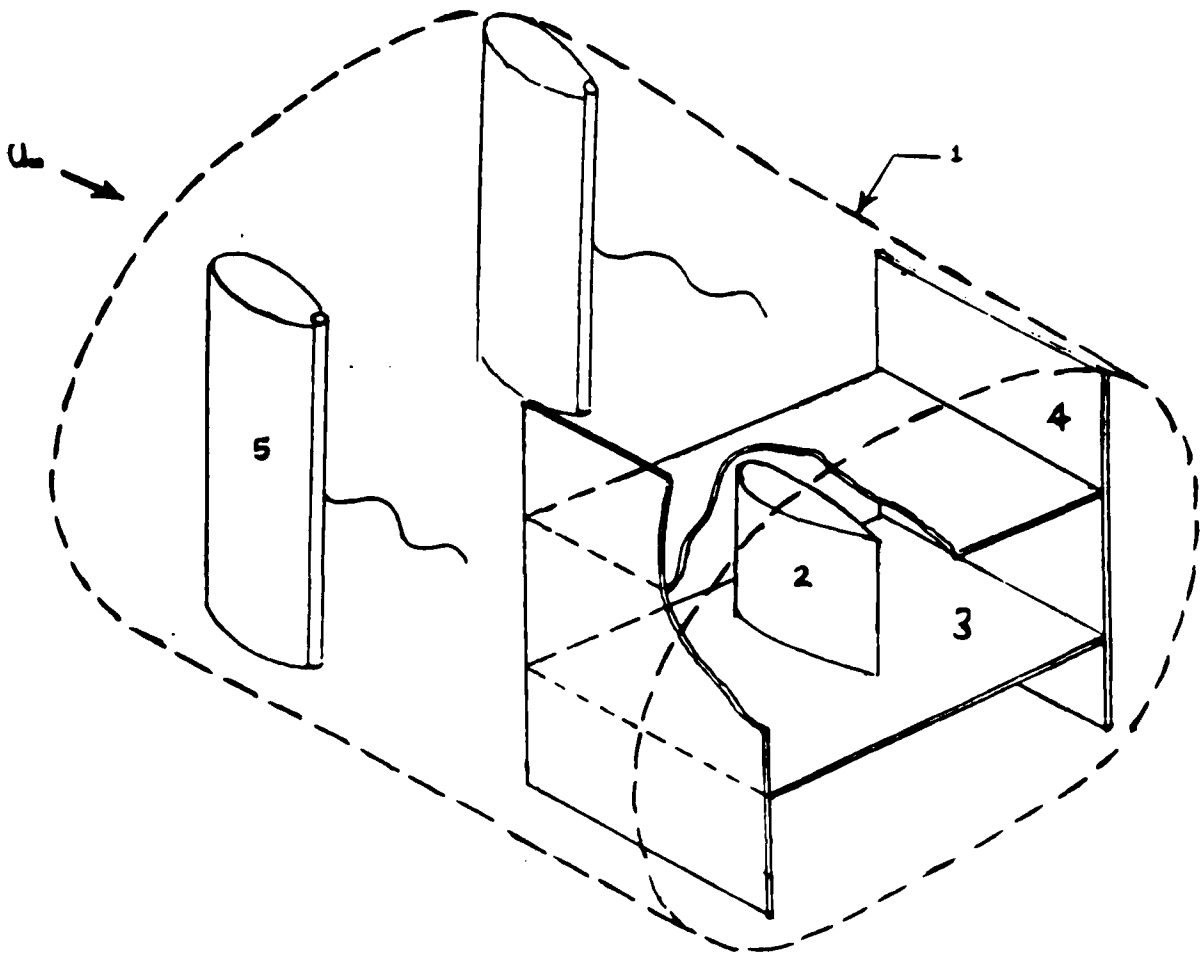

1) Test Section
2) NACA 0012 Airfoil
3) Sidewalls
4) Sidewall Supports
5) Gust Generator

FIGURE 4

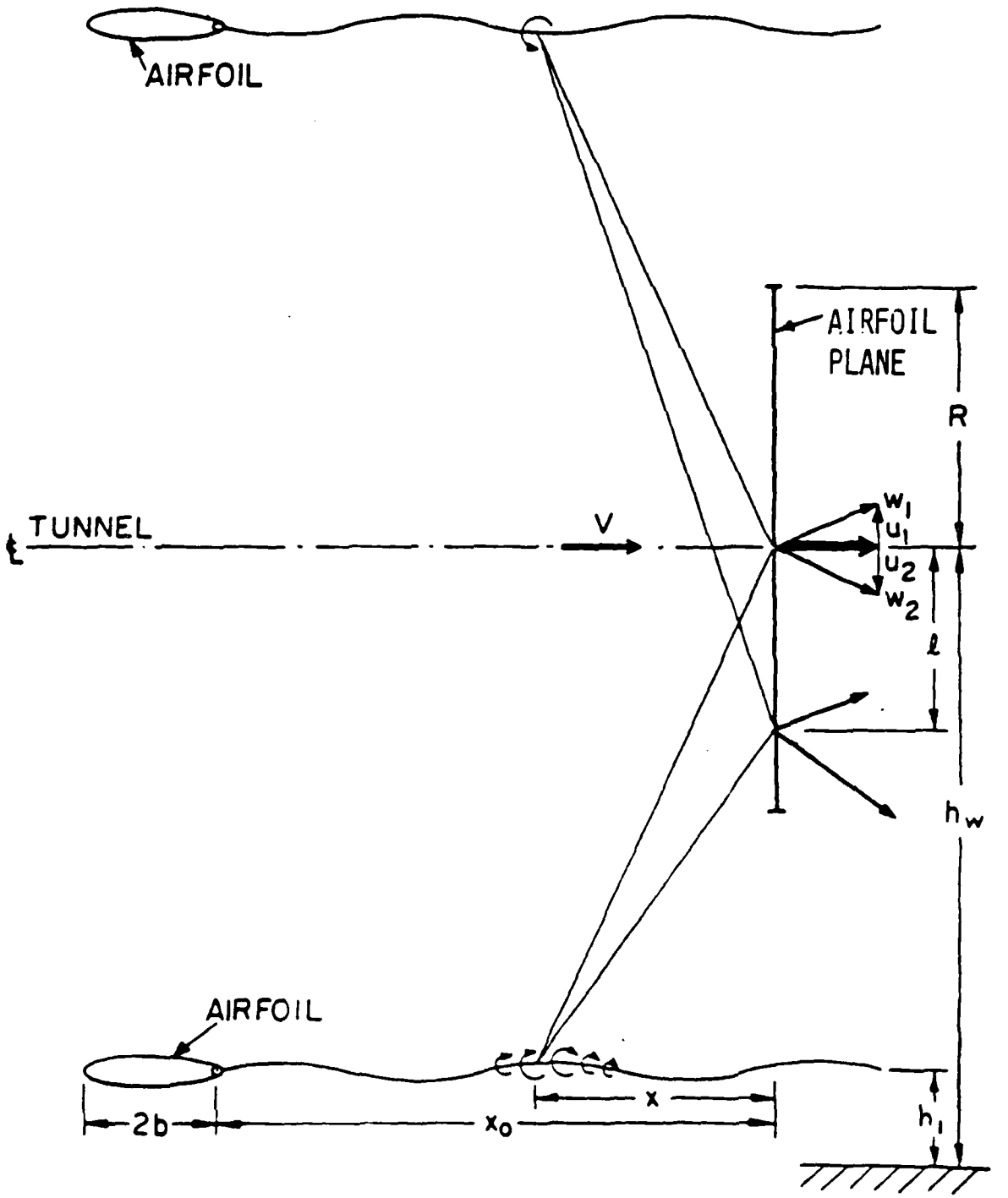

FIGURE 5 GUST GENERATOR GEOMETRY (REF 12.)

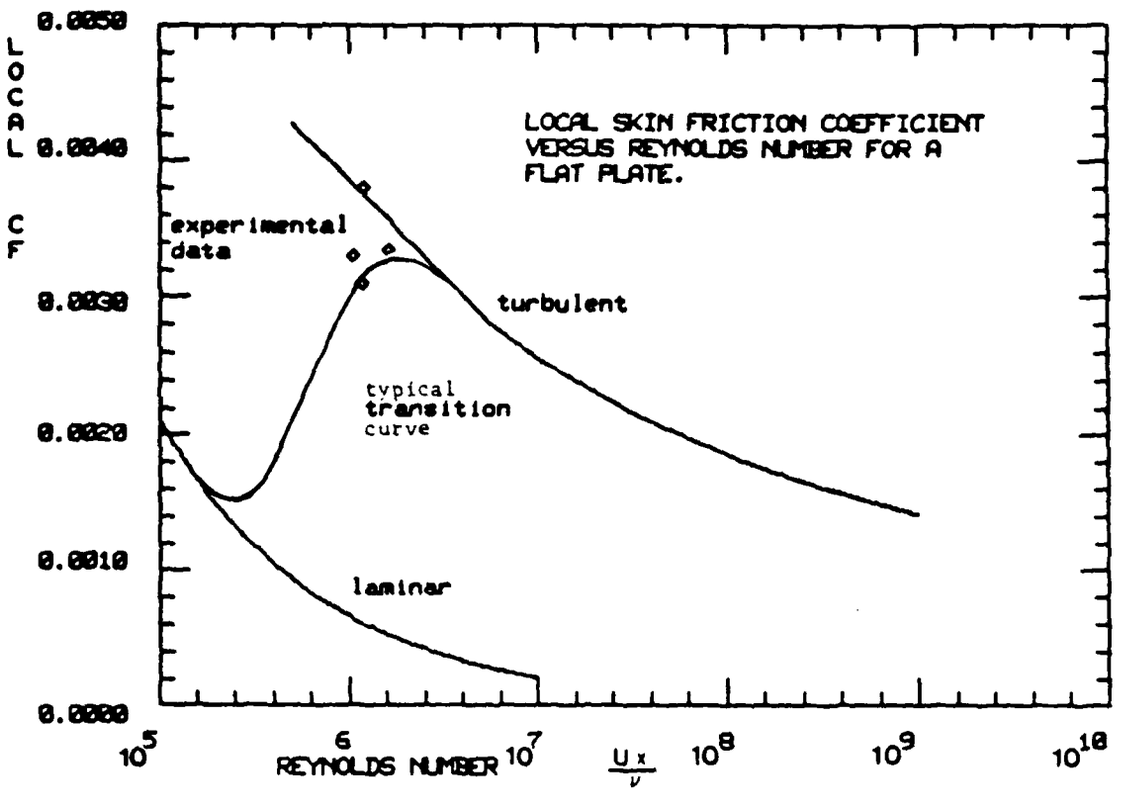

FIGURE 6 EXPERIMENTAL AND THEORETICAL FLAT PLATE RESULTS FOR LOCAL SKIN FRICTION COEFFICIENT VERSUS REYNOLDS NUMBER.

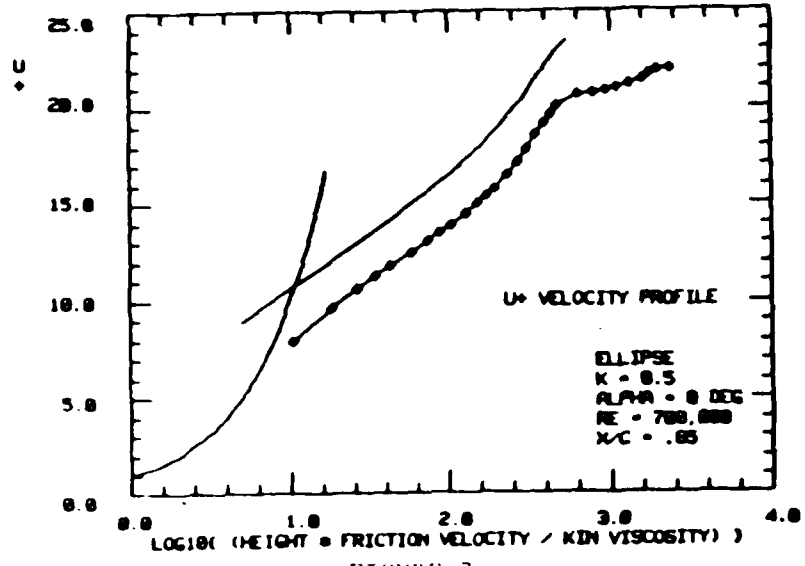

FIGURE 7

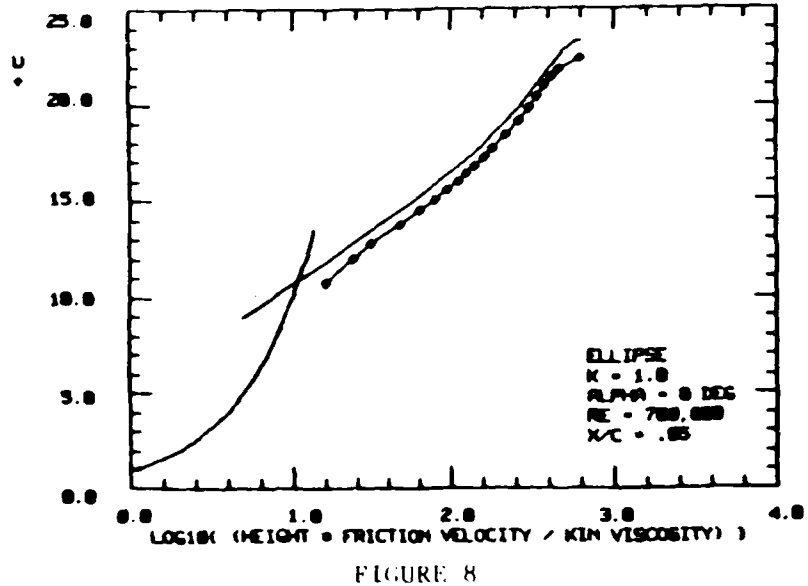

FIGURE 8

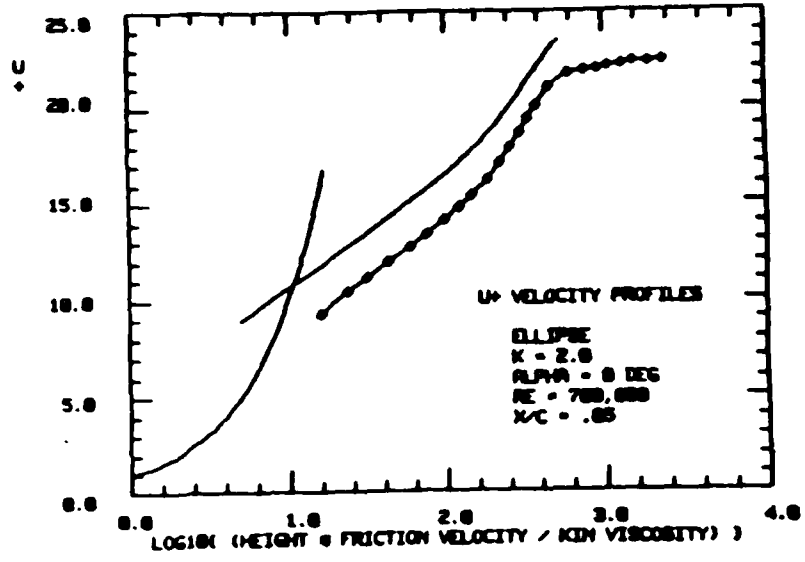

FIGURE 9

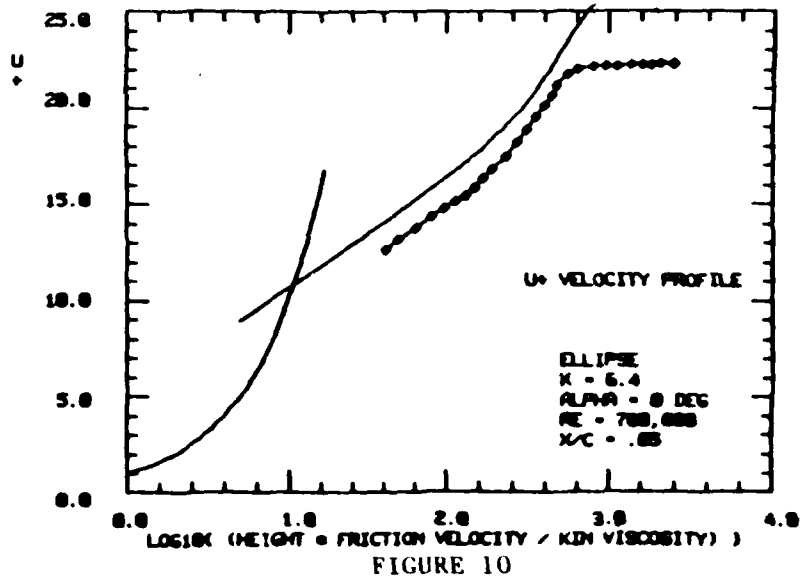

FIGURE 10

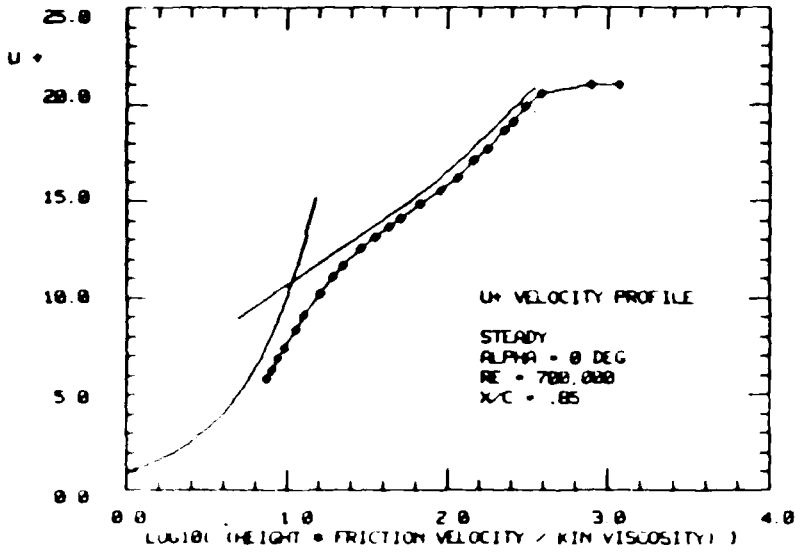

FIGURE 11

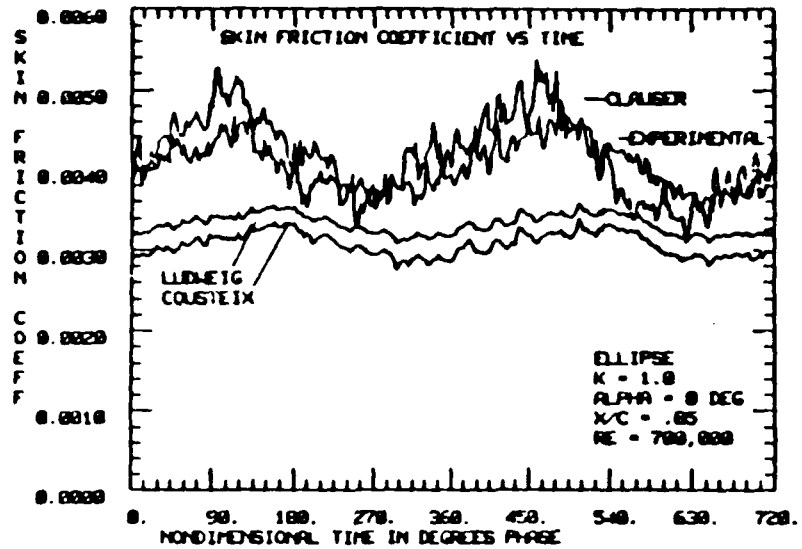

FIGURE 13

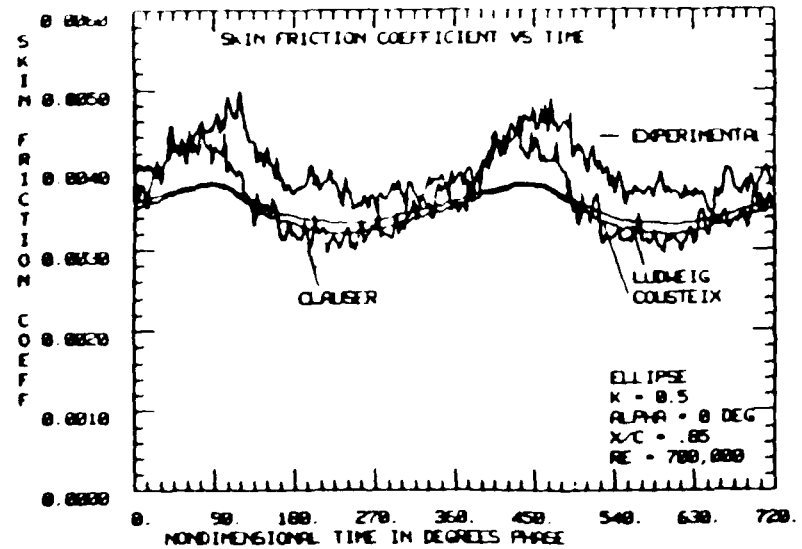

FIGURE 12

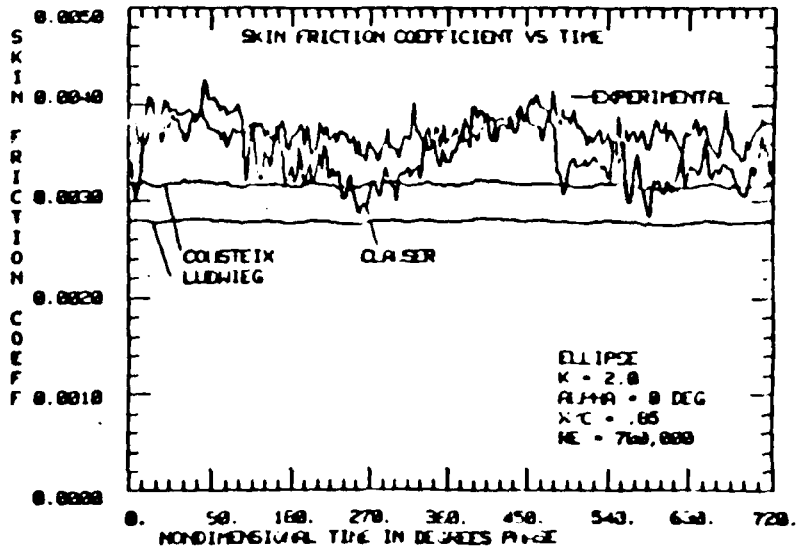

FIGURE 14

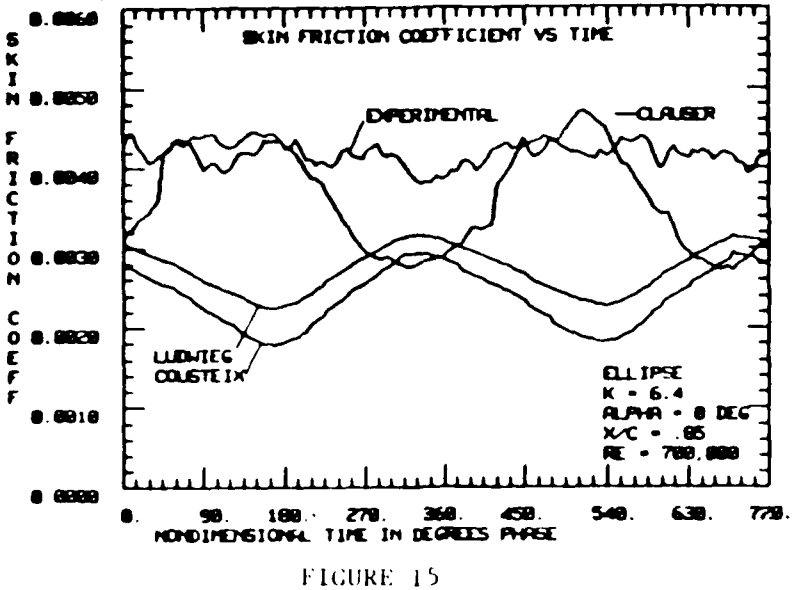

FIGURE 15

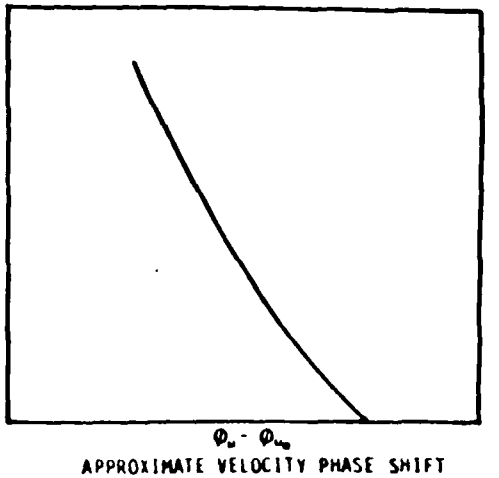

APPROXIMATE VELOCITY PHASE SHIFT
PROFILE FOR HIGH FREQUENCY

FIGURE 17

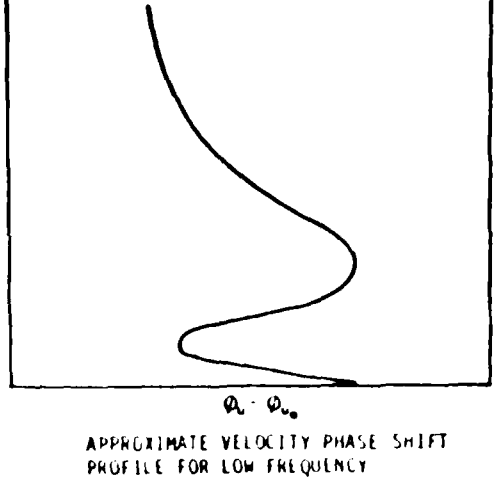

APPROXIMATE VELOCITY PHASE SHIFT
PROFILE FOR LOW FREQUENCY

FIGURE 16

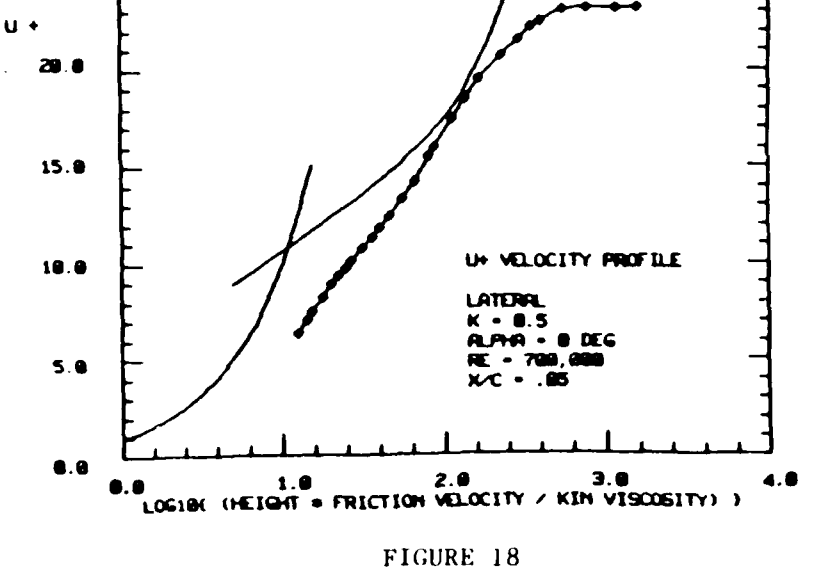

FIGURE 18

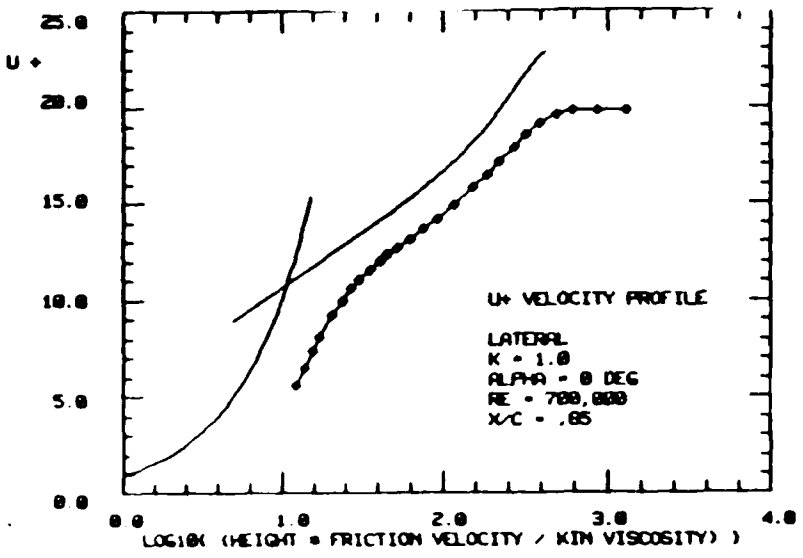

FIGURE 19

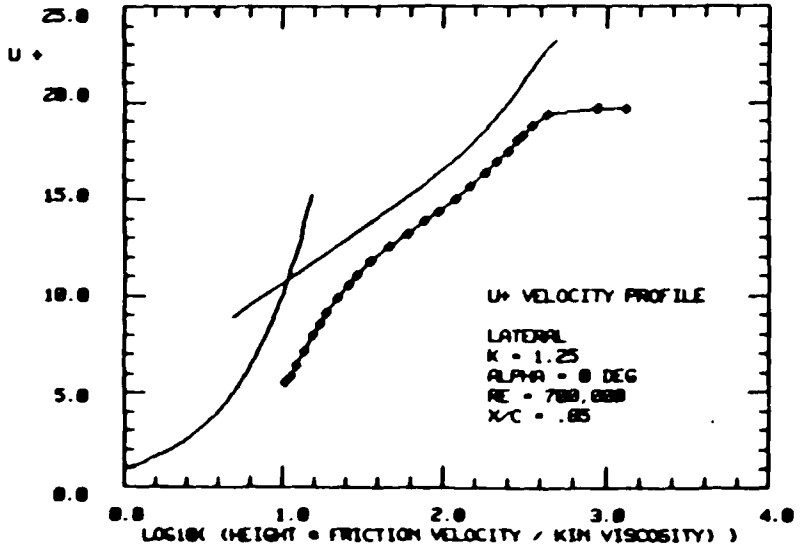

FIGURE 20

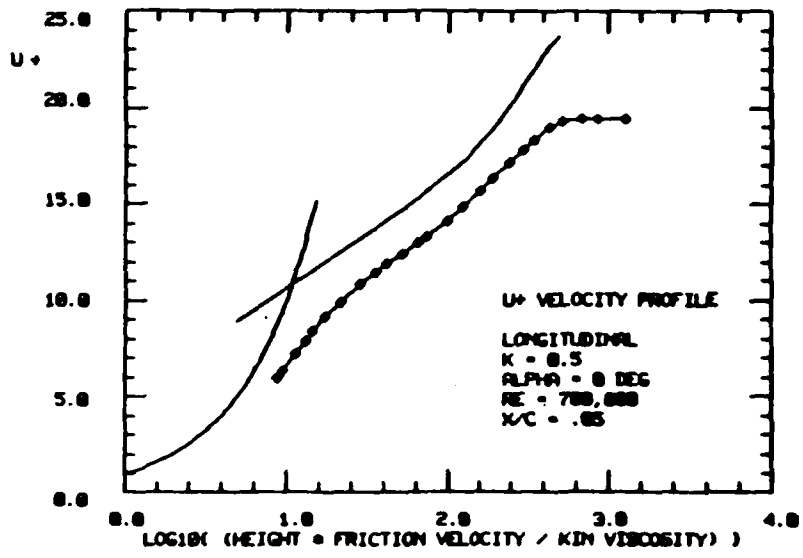

FIGURE 21

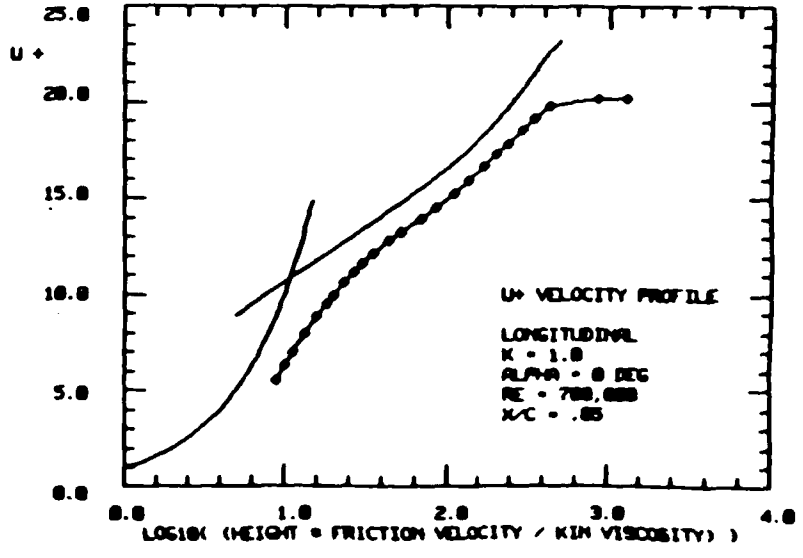

FIGURE 22

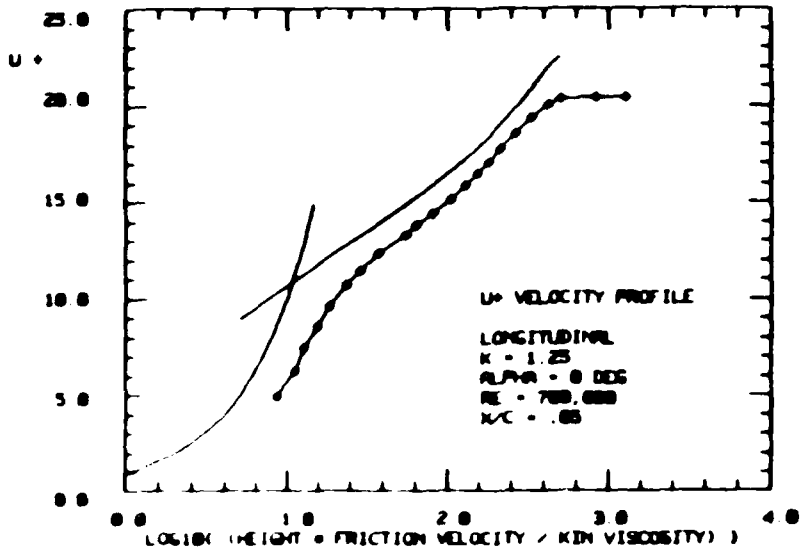

FIGURE 24

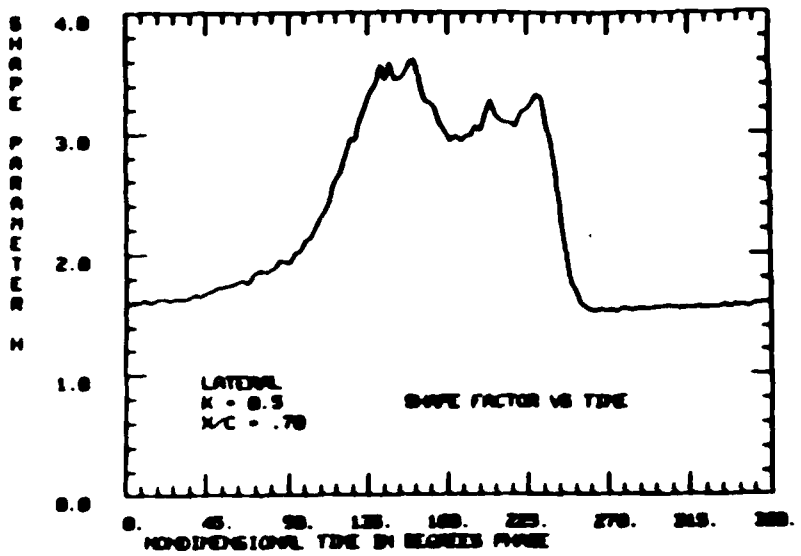

FIGURE 25

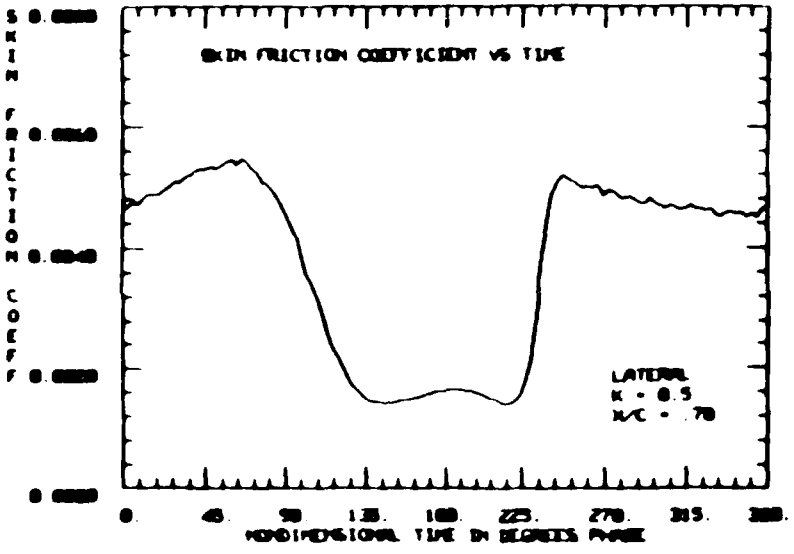

FIGURE

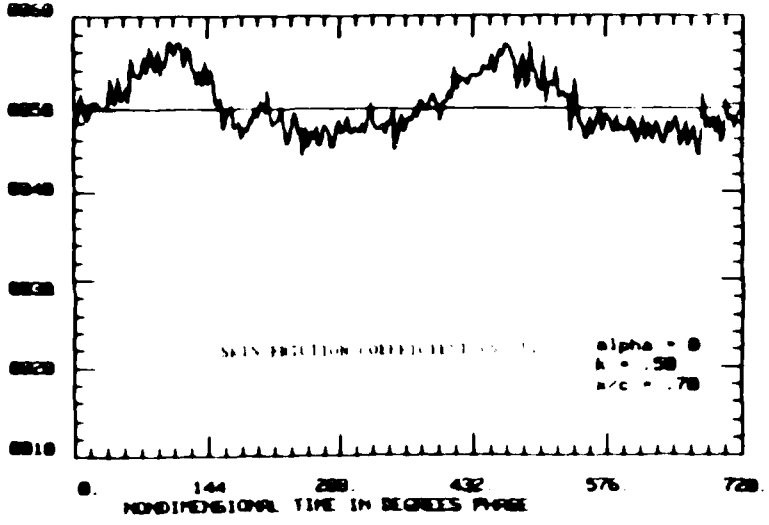

FIGURE 26

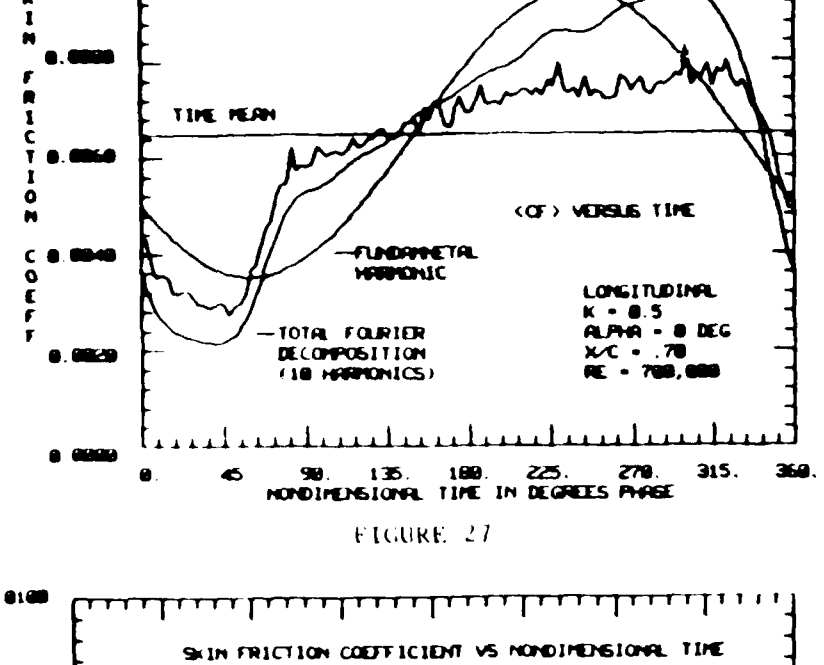

FIGURE 27

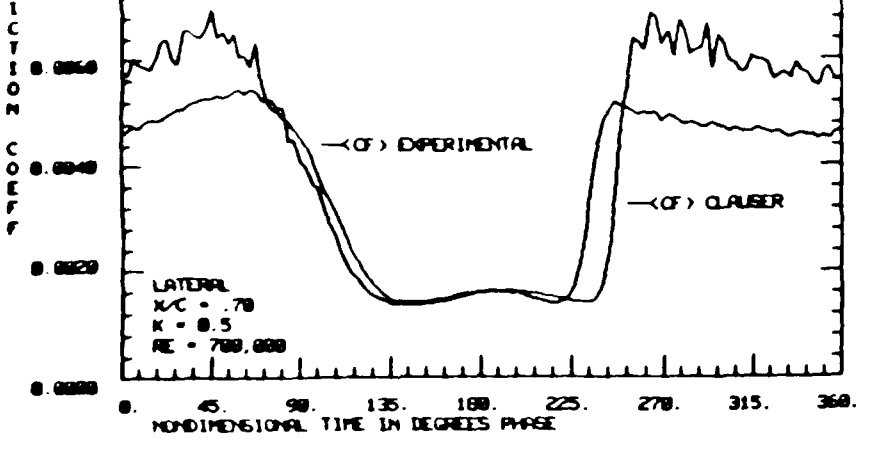

FIGURE 28

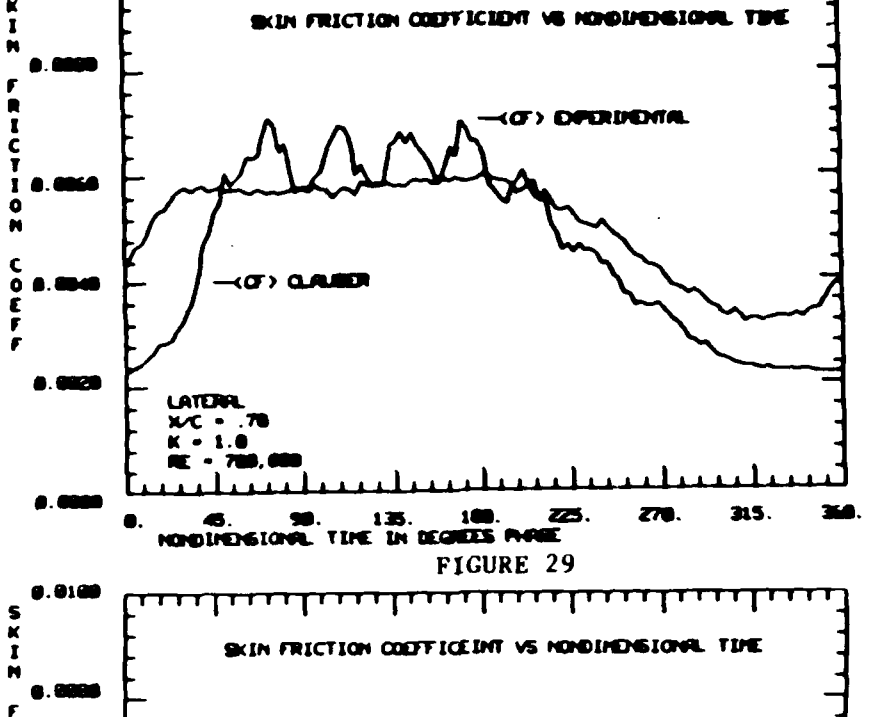

FIGURE 29

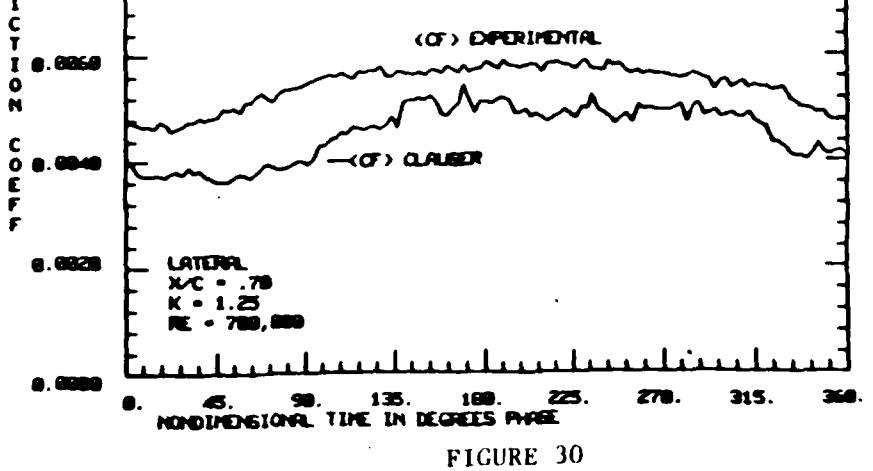

FIGURE 30

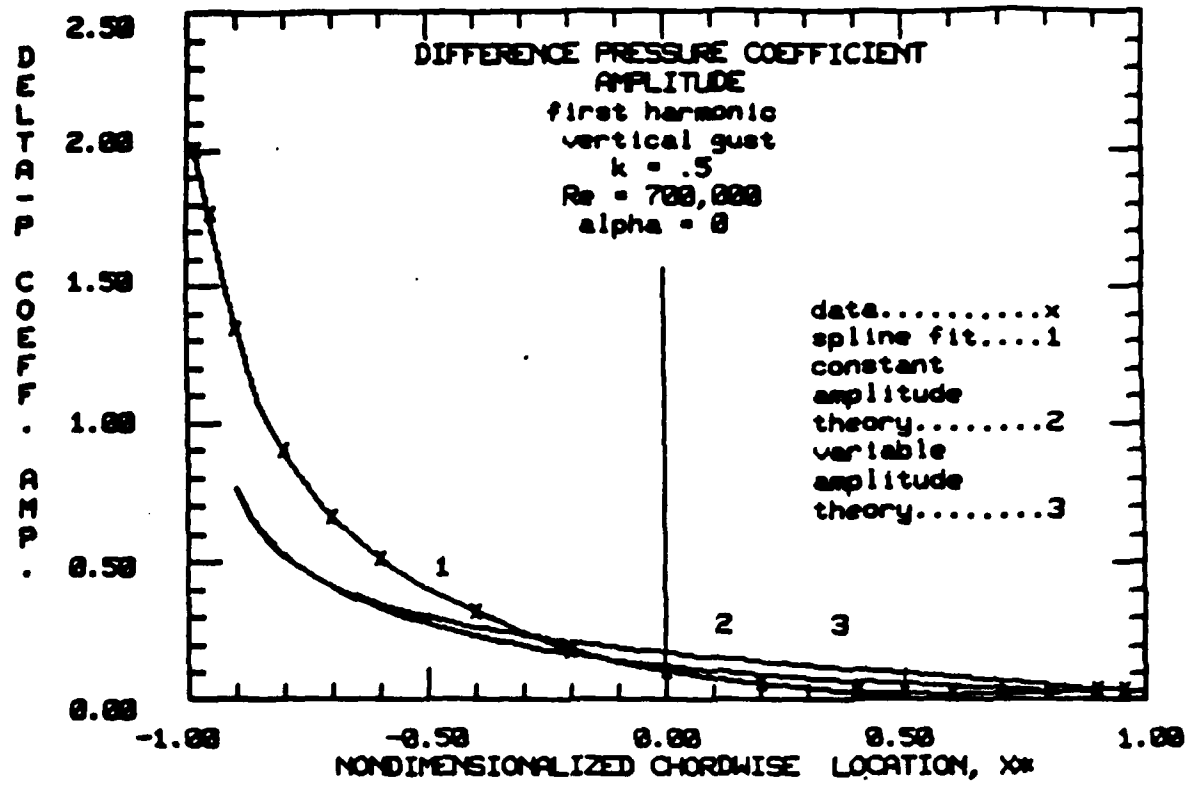

FIGURE 31

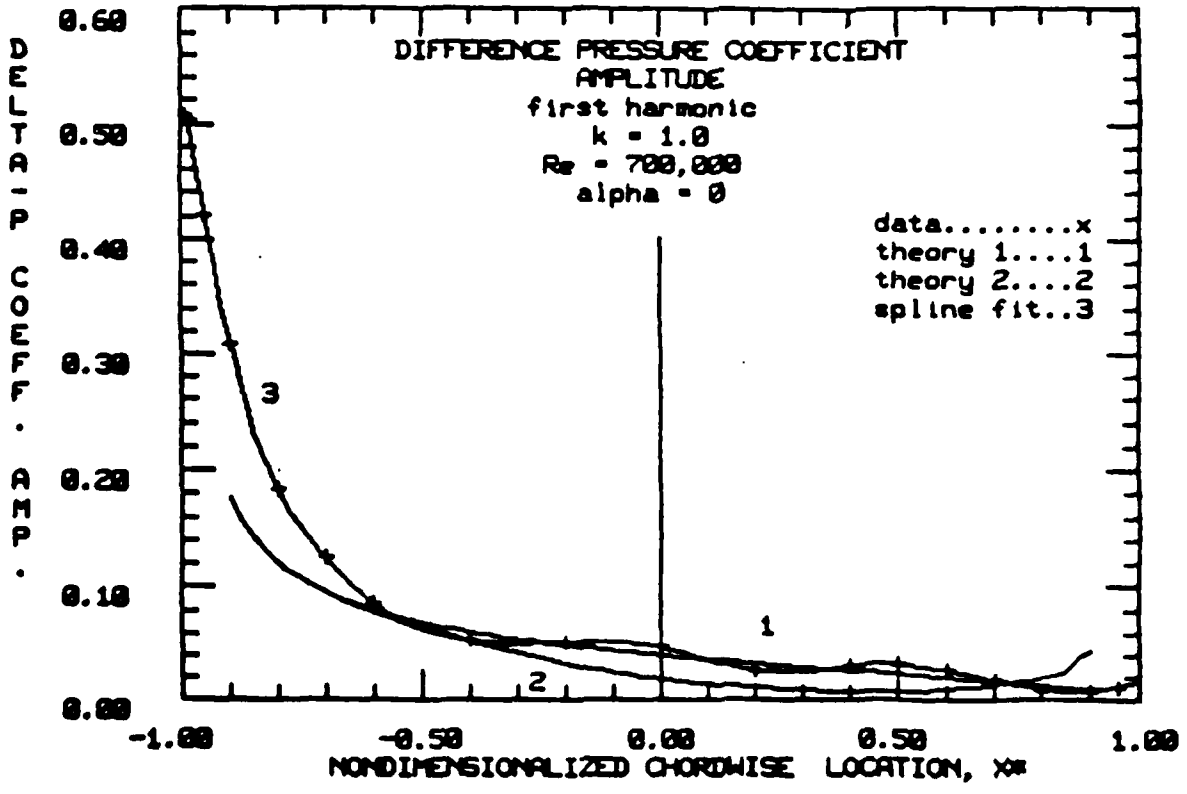

FIGURE 32

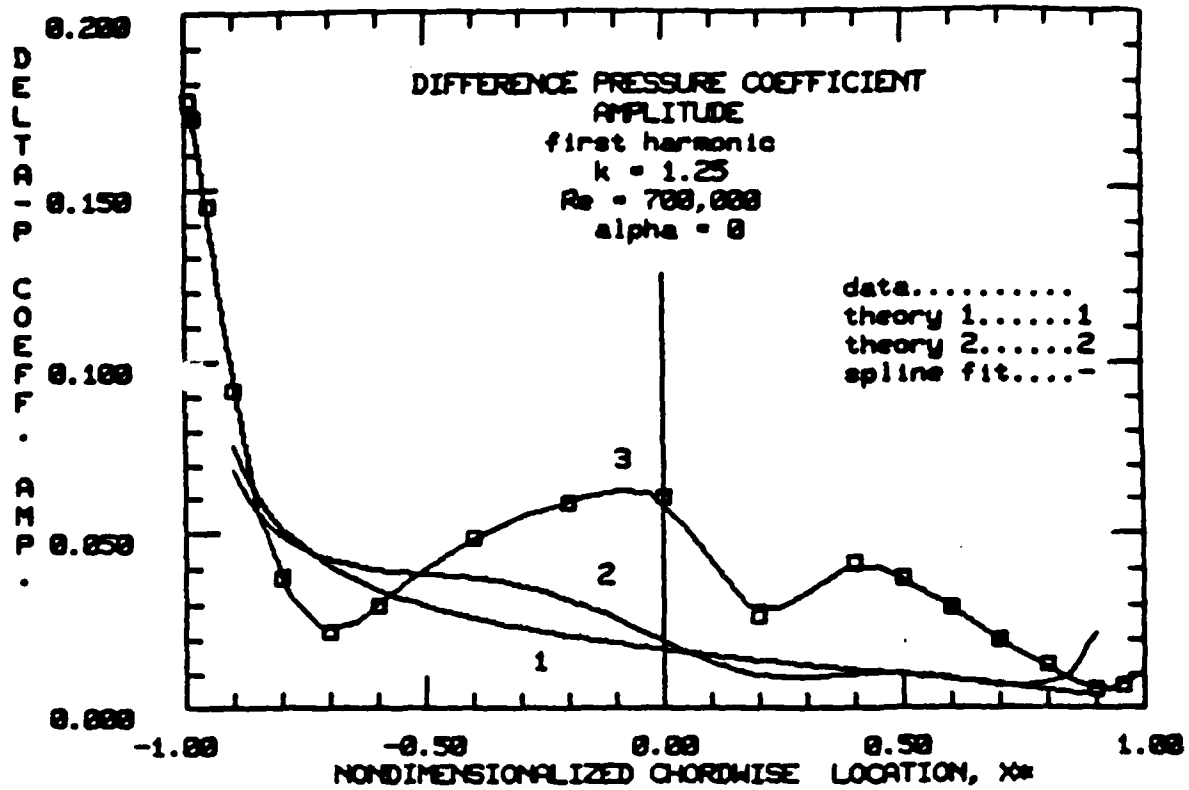

FIGURE 33

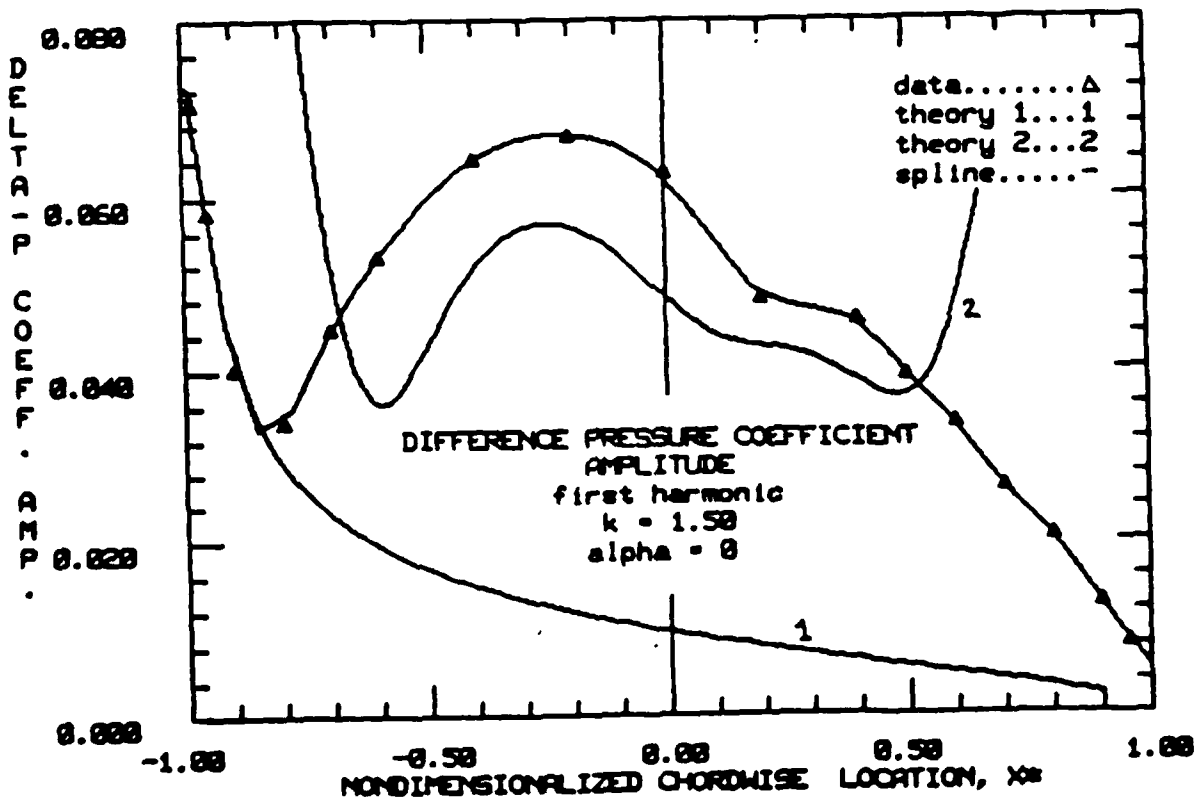

FIGURE 34

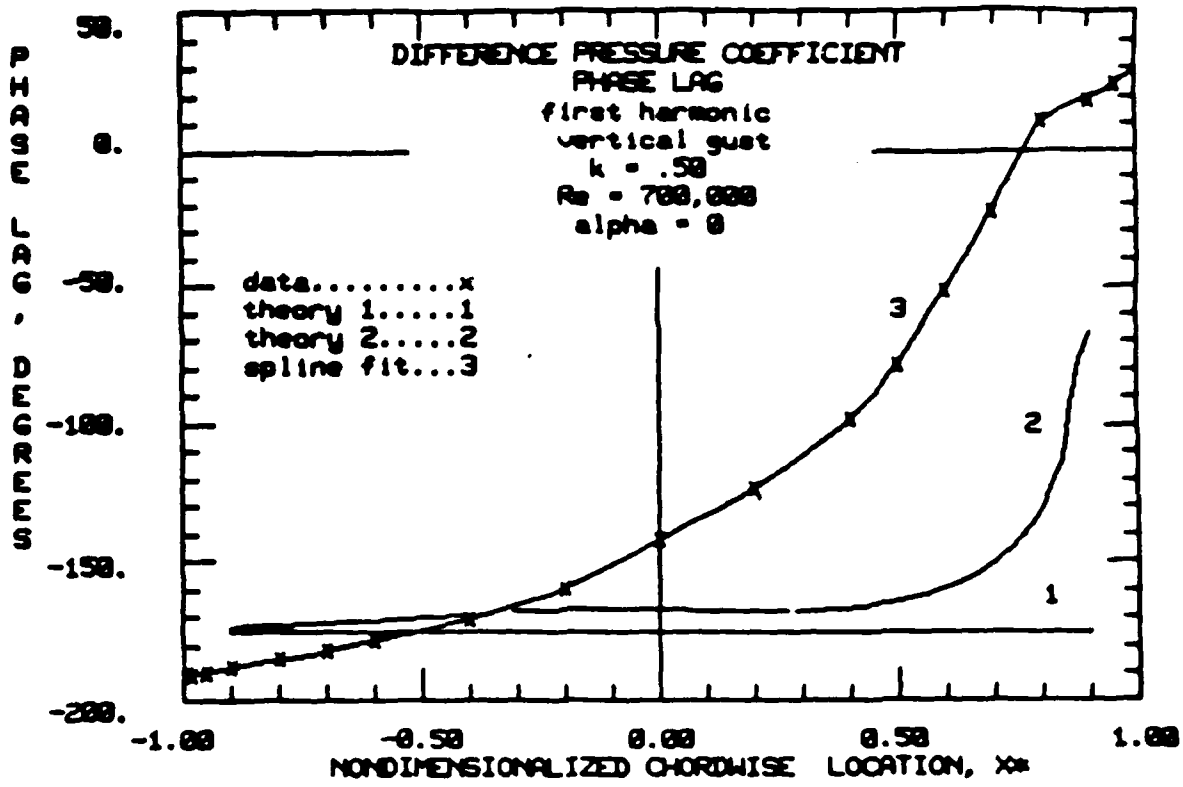

FIGURE 35

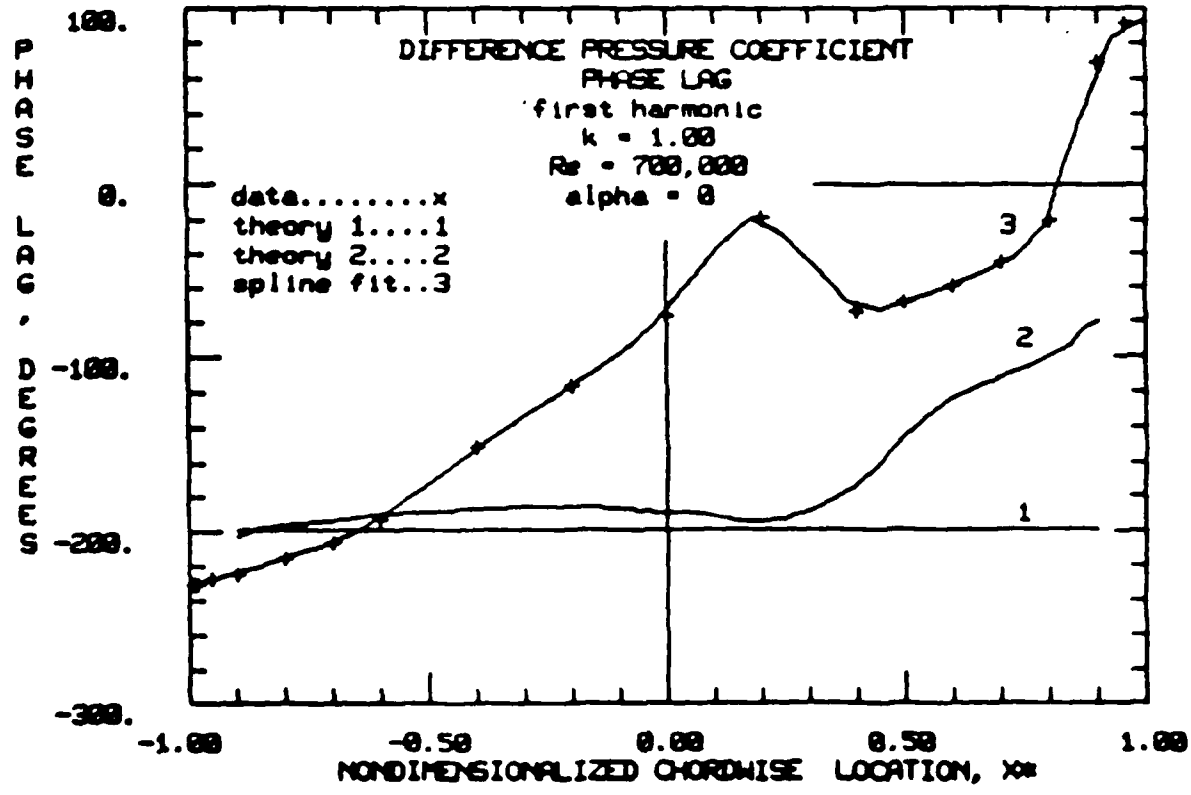

FIGURE 36

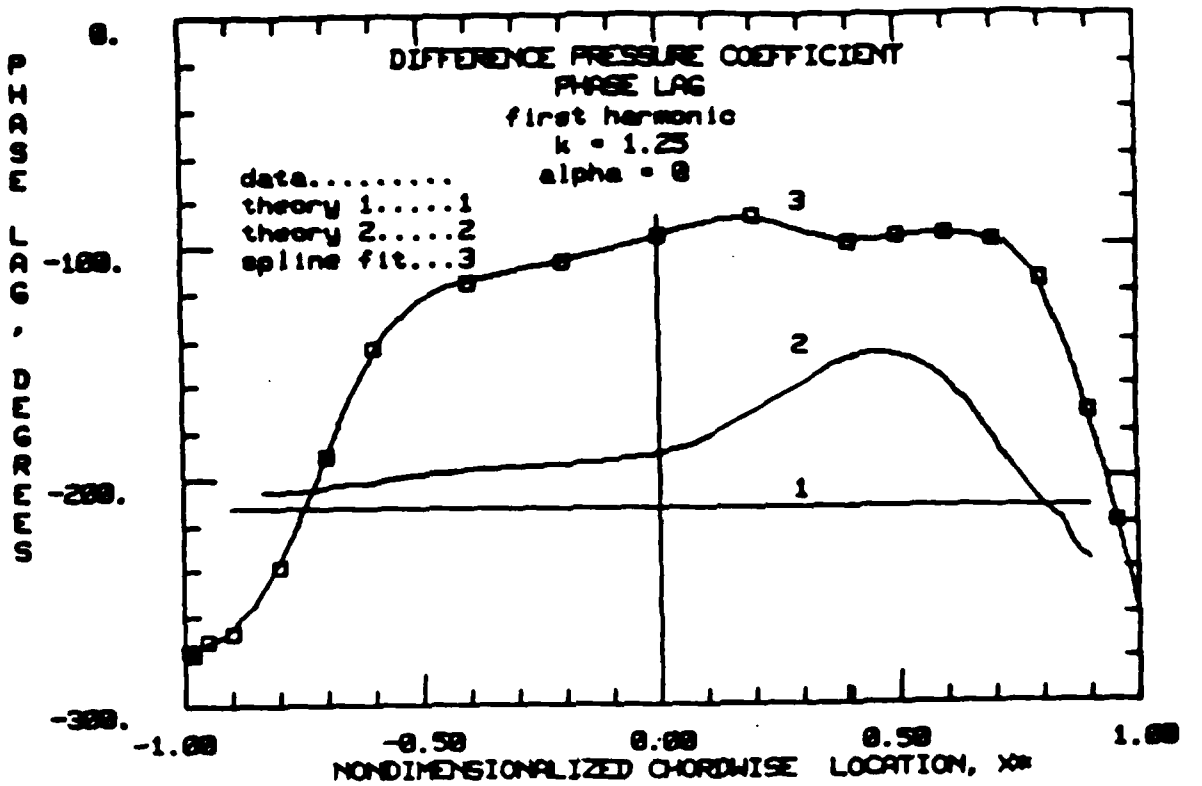

FIGURE 37

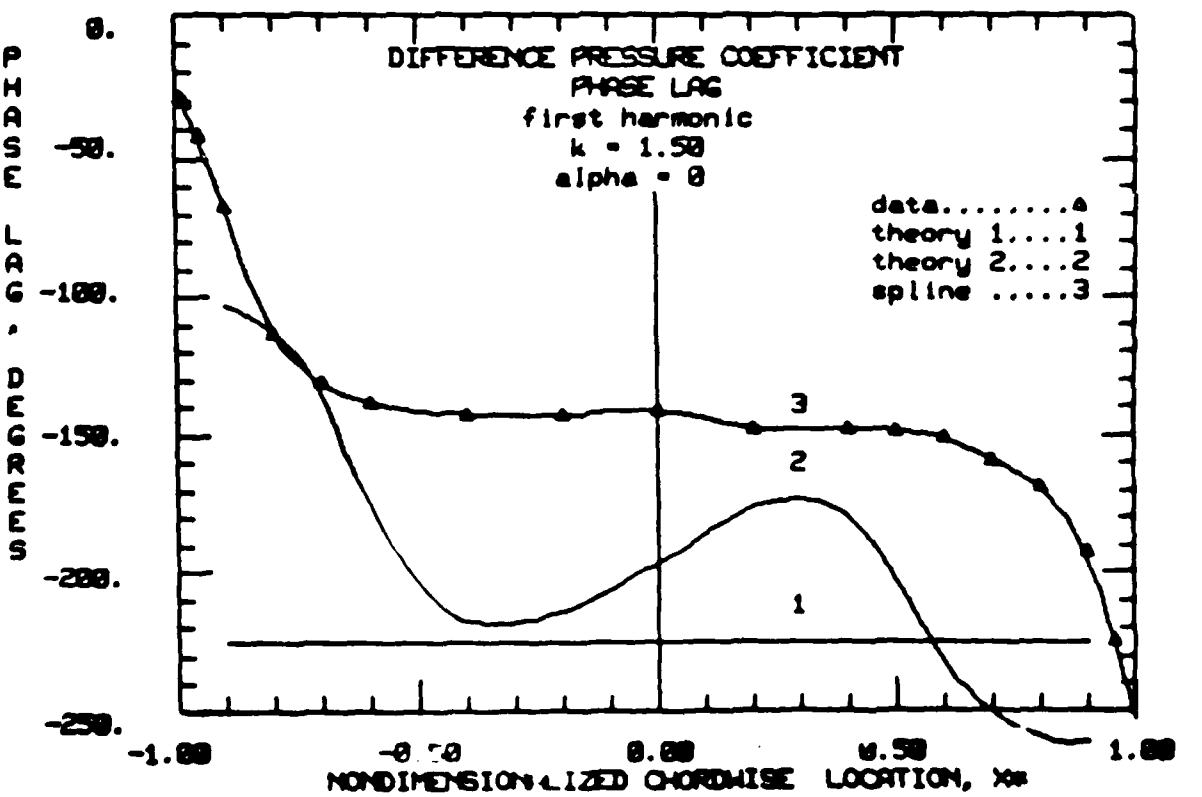

FIGURE 38

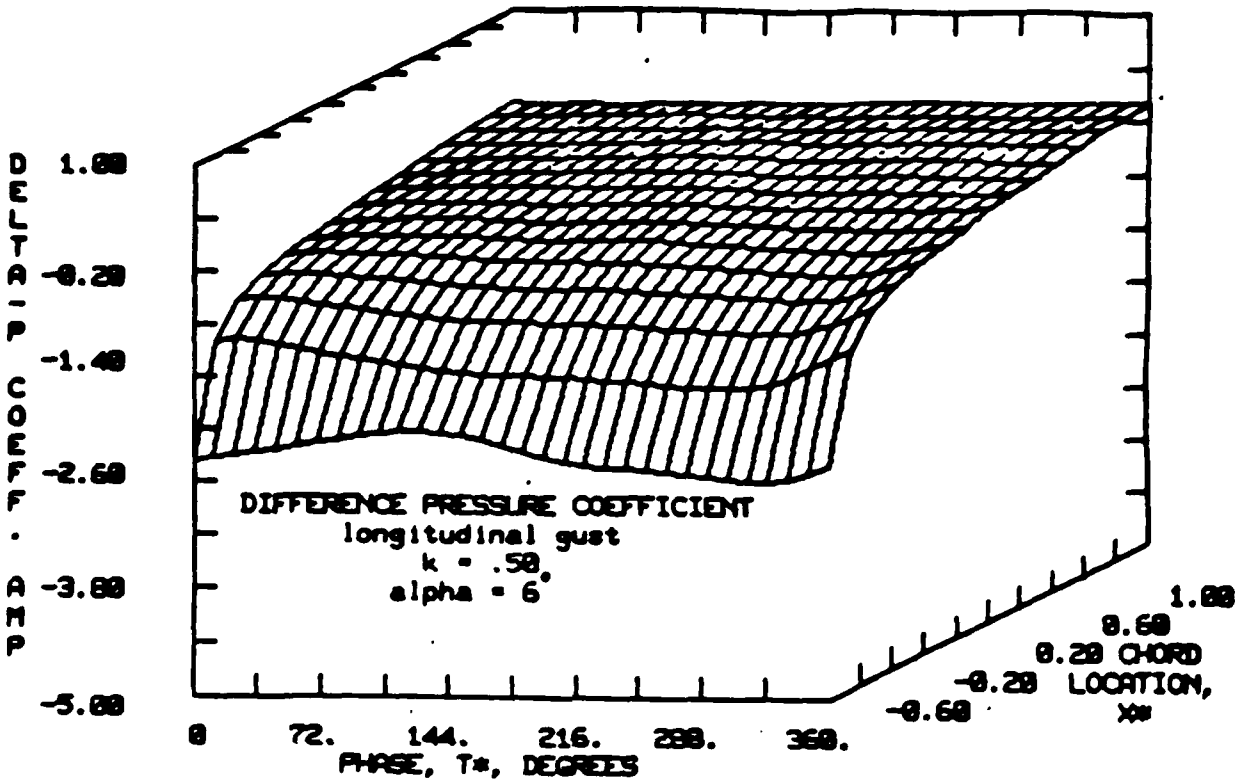

FIGURE 39

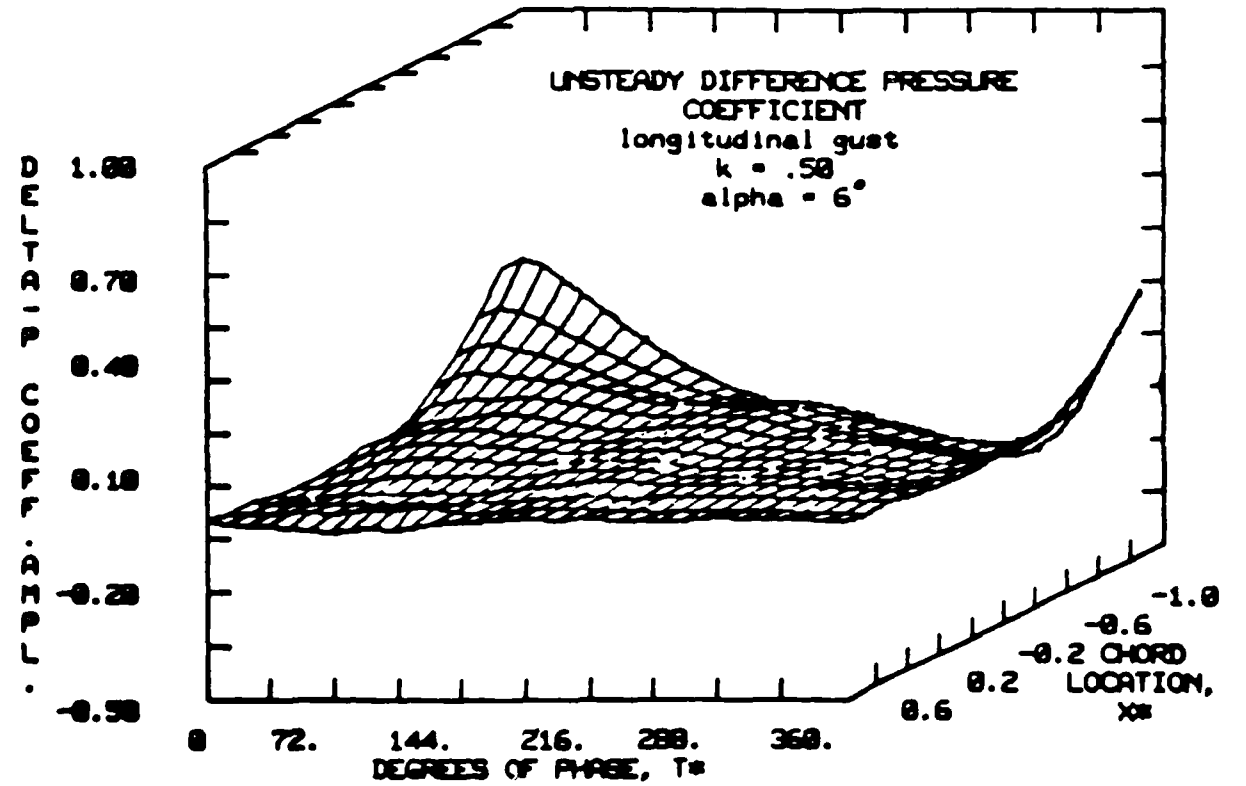

FIGURE 40

END

5-81

DTIC